

**GENERAL OPTICAL BEAM FORMULATION AND THEIR PROPAGATION
IN ATMOSPHERIC OPTICAL TELECOMMUNICATION LINKS**

**A THESIS SUBMITTED TO
THE GRADUATE SCHOOL OF NATURAL AND APPLIED
SCIENCES OF
ÇANKAYA UNIVERSITY**

**BY
CANAN YAZICIOĞLU**

**IN PARTIAL FULFILLMENT OF THE REQUIREMENTS FOR THE
DEGREE OF
MASTER OF SCIENCE
IN
THE DEPARTMENT OF
ELECTRONIC AND COMMUNICATION ENGINEERING**

JUNE 2007

Title of the Thesis : General Optical Beam Formulation and Their Propagation
in Atmospheric Optical Telecommunication Links

Submitted by Canan Yazıcıoğlu

Approval of the Graduate School of Natural and Applied Sciences, Çankaya
University



Prof. Dr. Yurdahan GÜLER
Director

I certify that this thesis satisfies all the requirements as a thesis for the degree of
Master of Science.



Prof. Dr. Yahya Kemal BAYKAL
Head of Department

This is to certify that we have read this thesis and that in our opinion it is fully
adequate, in scope and quality, as a thesis for the degree of Master of Science.



Prof. Dr. Yahya Kemal BAYKAL
Supervisor

Examination Date : 12.06.2007

Examining Committee Members

Prof. Dr. Yahya Kemal BAYKAL (Çankaya Univ.)



Prof. Dr. Erdem YAZGAN (Hacettepe Univ.)




Assoc. Prof. Dr. Yusuf Ziya UMUL (Çankaya Univ.)



STATEMENT OF NON-PLAGIARISM PAGE

I hereby declare that all information in this document has been obtained and presented in accordance with academic rules and ethical conduct. I also declare that, as required by these rules and conduct, I have fully cited and referenced all material and results that are not original to this work.

Name, Last Name : Canan Yazıcıoğlu
Signature : 
Date : 12.06.2007

ABSTRACT

GENERAL OPTICAL BEAM FORMULATION AND THEIR PROPAGATION IN ATMOSPHERIC OPTICAL TELECOMMUNICATION LINKS

YAZICIOĞLU, Canan

M.S., Department of Electronic and Communication Engineering

Supervisor: Prof. Dr. Yahya Kemal BAYKAL

June 2007, 77 pages

In this thesis, we have developed a general source beam to combine many types of different beams such as Bessel, Bessel Gaussian, Laguerre, Laguerre Gaussian, Ince Gaussian, dark hollow, bottle, super Gaussian, Lorentz, flat-topped, Hermite-sinusoidal-Gaussian, sinusoidal-Gaussian like cos-Gaussian, sine-Gaussian, cosh-Gaussian, sinh-Gaussian, annular and their higher order modes with their truncated, elegant and elliptical versions in a single expression. Also we developed a Matlab code to plot intensity distributions at source and receiver. Using this Matlab code and the general source beam formulation, all the mentioned beams' source equations are obtained, compared with their existing forms in the literature and intensity patterns of some of them are plotted at source plane. Using a part of this formulation and the Matlab simulation, intensity is calculated and plotted intensity distributions of Hermite-sinusoidal-Gaussian, sinusoidal-Gaussian, annular and higher-order annular beams at different propagation distances in atmospheric turbulence.

Keywords: Free Space Optics, Atmospheric Turbulence, Intensity.

ÖZ

GENEL OPTİK IŞIK HÜZMESİ FORMÜLASYONU VE ATMOSFERİK OPTİK TELEKOM LİNKLERİNDEKİ YAYILIMLARI

Yazıcıoğlu, Canan

Yüksek Lisans, Elektronik ve Haberleşme Mühendisliği Anabilim Dalı

Tez Yöneticisi: Prof. Dr. Yahya Kemal Baykal

Haziran 2007, 77 sayfa

Bu tezde, Bessel, Bessel Gauss, Laguerre, Laguerre Gauss, Ince Gauss, dark hollow, bottle, super Gauss, Lorentz, düz tepeli, Hermite-sinusoidal-Gauss, sinusoidal-Gauss (cos-Gauss, sine-Gauss, cosh-Gauss, sinh-Gauss), halkasal ışık hüzmeleri ve bunların yüksek dereceli durumları truncated, elegant ve eliptik versiyonları gibi ışık hüzmelerini genel bir kaynak ışık hüzmesi olarak geliştirdik. Ayrıca kaynak ve alıcı düzlemindeki ışık şiddeti dağılımını çizmek için bir Matlab programı yazdık. Bu Matlab programını ve genel kaynak hüzme formülünü kullanarak, tüm bahsedilen ışık hüzmelerinin kaynak denklemlerini elde ettik ve literatürdeki formlarıyla karşılaştırdık, bazı ışık hüzmelerinin ışık şiddeti dağılımını Matlab programını kullanarak kaynak düzleminde çizdirdik. Bu genel hüzme formülünün bir parçasını ve Matlab programını kullanarak Hermite-sinusoidal-Gauss, sinusoidal-Gauss, halkasal ve yüksek dereceli halkasal ışık hüzmelerinin ışık şiddeti dağılımını değişik yayılım uzaklıklarında atmosferik türbülans altında çizdirdik.

Anahtar Kelimeler: Serbest Uzay Optik İletişim, Atmosferik Türbülans, Işık Şiddeti.

ACKNOWLEDGEMENTS

I would like to express my sincere gratitude to Prof. Dr. Yahya BAYKAL for his supervision, special guidance, suggestions, and encouragement through the development of this thesis.

I would like to thank Assoc. Prof. Dr. Yusuf Ziya UMUL , Asst. Prof. Dr. Halil T. EYYUBOĞLU, Serap ALTAY ARPALI, and Çağrı İLLEEZ for their support and advises.

It is a pleasure to express my special thanks to my family for their constant support, patience and sincere love.

TABLE OF CONTENTS

STATEMENT OF NON PLAGIARISM.....	iii
ABSTRACT.....	iv
ÖZ.....	vi
ACKNOWLEDGEMENTS.....	viii
TABLE OF CONTENTS.....	ix
LIST OF TABLES.....	xi
LIST OF FIGURES.....	xii
LIST OF ABBREVIATIONS.....	xiv

CHAPTERS:

1. INTRODUCTION.....	1
1.1 Background.....	2
1.2 Objectives.....	3
1.3 Organization of the Thesis.....	3
2. EFFECTS OF THE ATMOSPHERE IN OPTICAL WAVE PROPAGATION..	4
2.1 Molecular and Aerosol Absorption.....	5
2.2 Molecular and Aerosol Scattering.....	5
2.3 Free-Space Propagation of Gaussian-Beam Waves.....	6
2.4 Atmospheric Turbulence and Extended Huygens-Fresnel Integral.....	9
2.4.1 Classical Turbulence and Kolmogorov Theory.....	9
2.4.2 Laser Beam Propagation and the Extended Huygens-Fresnel Integral.....	12
3. FORMULATION OF GENERAL SOURCE BEAM AND THE LIMITING CASE RESULTS.....	14

3.1 Limiting Cases.....	15
3.1.1 Bessel Beam.....	16
3.1.2 Bessel Gaussian Beam.....	17
3.1.3 Laguerre Beam.....	18
3.1.4 Laguerre Gaussian Beam.....	20
3.1.5 Ince Gaussian Beam.....	21
3.1.6 Dark Hollow Beam.....	23
3.1.7 Bottle Beam.....	25
3.1.8 Flat-toppe Beam.....	27
3.1.9 Super Gaussian Beam.....	29
3.1.10 Lorentz Beam.....	30
3.1.11 Hermite-sinusoidal-Gaussian Beams.....	31
3.1.11.1 Hermite-cosh-Gaussian Beam.....	34
3.1.11.2 Hermite-cos-Gaussian Beam.....	35
3.1.11.3 Hermite-sinh-Gaussian Beam.....	35
3.1.11.4 Cos-Gaussian Beam.....	36
3.1.11.5 Cosh-Gaussian Beam.....	37
3.1.11.6 Sine-Gaussian Beam.....	37
3.1.11.7 Sinh-Gaussian Beam.....	38
3.1.11.8 Higher-order Annular Beam.....	38
3.1.12 Elegant Laguerre Gaussian Beam.....	39
3.1.13 Elliptical Gaussian Beam.....	40
4. FORMULATION AND RESULTS FOR THE AVERAGE RECEIVED INTENSITY OF GENERAL BEAMS IN ATMOSPHERIC TURBULENCE.....	41
5. CONCLUSIONS.....	56
REFERENCES.....	R1

LIST OF TABLES

TABLES

Table 3.1 Parameters for Hermite Gaussian Beams.....	33
Table 3.2 Parameters for Sinosoidal Gaussian Beams.....	36

LIST OF FIGURES

FIGURES

Figure 2.1 Electromagnetic Spectrum.....	6
Figure 2.2 Amplitude profile of a Gaussian beam.....	9
Figure 2.3 Kolmogorov cascade theory of turbulence, where L_0 denotes the outer scale and l_0 is the inner scale. Eddies between scale sizes l_0 and L_0 form the inertial subrange.....	12
Figure 3.1 Intensity distribution of Bessel beam the source plane.....	17
Figure 3.2 Intensity distribution of Laguerre Gaussian beam at the source plane with mode orders (0,1).....	21
Figure 3.3 Intensity distribution of dark hollow beam at the source plane.....	25
Figure 3.4 Bottle beam intensity at the source plane.....	27
Figure 3.5 Flat-topped intensity at the source plane with $N_f = 10$	28
Figure 3.6 Super Gaussian beam intensity at the source plane for $N_s = 8$	30
Figure 3.7 Lorentz beam intensity at the source plane.....	31
Figure 3.8 Intensity distribution of Hermite-sine-Gaussian beam with $n = 1, m = 0$ at the Source plane.....	34
Figure 4.1 Intensity distribution of Hermite-sine-Gaussian beam $n = 1, m = 0$, at $L=0, 2, 5, 20$ km.....	46
Figure 4.2 Intensity distribution of Hermite-cosh-Gaussian beam with $n = 1, m = 1$, at $L=0, 2, 5, 20$ km.....	47

Figure 4.3 Intensity distribution of Hermite-cosine-Gaussian beam with $n = 1, m = 1$, at $L = 0, 2, 5, 20$ km.	48
Figure 4.4 Intensity distribution of a Hermite-sinh-Gaussian beam with $n = 1, m = 0$, at $L = 0, 2, 5, 20$ km.	49
Figure 4.5 Intensity distribution of cosine-Gaussian beam with $n = 0, m = 0$, at $L = 0, 2, 5, 20$ km.	50
Figure 4.6 Intensity distribution of cosh-Gaussian beam with $n = 0, m = 0$, at $L = 0, 2, 5, 20$ km.	51
Figure 4.7 Intensity distribution of a sine-Gaussian beam with $n = 1, m = 0$, at $L = 0, 2, 5, 20$ km.	52
Figure 4.8 Intensity distribution of a sinh-Gaussian beam with $n = 0, m = 0$, at $L = 0, 2, 5, 20$ km.	53
Figure 4.9 Intensity distribution of annular beam with $n = 0, m = 0$, at $L = 0, 2, 5, 20$ km.	54
Figure 4-10 Intensity distribution of a higher order annular beam with $n = 1, m = 0$, at $L = 0, 2, 5, 20$ km.	55

LIST OF ABBREVIATIONS

RF	Radio Frequency
FSO	Free Space Optics
IR	Infrared
TEM	Transverse Electromagnetic

CHAPTER 1

INTRODUCTION

1.1 Background

With the recent developments in semiconductor technology, free space optical or optical wireless communication has become an attractive alternative to optical fiber communications or radio frequency (RF) systems. Historically, Free Space Optics (FSO) was first demonstrated by Alexander Graham Bell in the late nineteenth century. Bell's FSO experiment converted voice sounds into telephone signals and transmitted them between receivers through free air space along a beam of light for a distance of some 600 feet. Because it did not require wires for transmission, Bell considered this optical technology his perfect invention. Although Bell's invention never became commercially real, it demonstrated the basic principle of optical communications [1].

From late 1950's to early 1960's several scientists developed lasers. In the mid-1960's NASA initiated experiments to utilize the laser as a means of communication between the Goddard Space Flight Center and the Gemini-7 orbiting space capsule. Germany, France and Japan made significant advancements in FSO for satellite communications.

FSO communications refer to the transmission of modulated visible or infrared (IR) beams through the atmosphere to obtain optical communications. Like fiber, FSO uses lasers to transmit data, but instead of enclosing the data stream in a glass fiber, it is transmitted through the air. FSO uses laser technology to send optical signals through the air using lenses and mirrors to focus and redirect the beams and send data from one chip to another. And unlike radio frequencies, FSO technology does not require a spectrum license. An FSO system offers much higher data rates when

underground fiber. It offers a flexible networking solution. Only FSO provides the essential combination of qualities required to bring the traffic to the optical fiber backbone. Since FSO transceivers can transmit and receive through windows, it is possible to mount FSO systems inside buildings, reducing the need to compete for roof space, simplifying wiring and cabling, and permitting the equipment to operate in a very favorable environment. One of the essential points for FSO is the line of sight between the two ends of the link. There should be no obstructions such as trees or buildings between the transceiver units [2].

There are certain fundamental effects concerning optical wave propagation. Among these are diffraction, atmospheric attenuation, atmospheric absorption, atmospheric turbulence and thermal blooming. Except for thermal blooming, which is a nonlinear effect, the other effects are considered linear. Atmospheric conditions affect beams' intensity at the receiver. The purpose of all the studies is to reduce these negative effects. Beam types and the intensities of these beams have been investigated when they propagate in the absence of turbulence. Durnin calculated the intensity of Bessel and Bessel-Gauss beams on-axis. [3]. Kogelnik studied Laguerre-Gaussian beams after the invention of laser [4]. Bandres and Vega demonstrated the existence of the Ince-Gaussian beams that constitute the third complete family of exact and orthogonal solutions of the paraxial wave equation [5]. Yin, Zhu, Wang and Yin studied on dark-hollow beams [6]. Arlt and Padgett studied the optical bottle beams which are obtained by the superposition of two Laguerre-Gaussian modes that are phased so that they interfere destructively to give a beam focus that is surrounded in all directions by regions of higher intensity [7]. Jiang studied on super-Gaussian functions and calculated the intensity [8]. Gawhary introduced a new kind of tri-dimensional scalar optical beams which are called Lorentz beams because of the form of their transverse pattern in the source plane [9]. Gori studied on flat beams [10]. Saghafi and Sheppard studied the elegant Laguerre-Gaussian beams [11]. Lin, Wang, Alda, and Bernabeu studied the elliptical Gaussian beam [12]. Also it is calculated off-axis intensity values for Gaussian, cos-Gauss, cosh-Gauss, sine-Gauss, sinh-Gauss, annular and their higher

order modes [13]. A time factor of $e^{i\omega t}$ is assumed and suppressed throughout the thesis.

1.1 Objectives

It is the aim of this work to combine the existing optical beam fields in a single general beam formula and plot the intensity distributions at the exit plane of the laser for many types of specific beams, such as Bessel-Gaussian, Laguerre-Gaussian, Laguerre, Ince-Gaussian, annular, bottle, super Gaussian, Lorentz, flat-topped, Hermite-sinusoidal-Gaussian and their truncated, elegant and elliptical versions. In the second part of the thesis, a more limited form of this general beam is used to examine the propagation characteristics in a turbulent atmosphere. Within this context, average intensity at the receiver plane is calculated and the effect of various beam profiles on the variation of the received average intensity profiles are examined in a turbulent atmosphere.

1.2 Organization of the Thesis

This thesis comprises five chapters. Chapter 1 is an introduction to this study which contains the objective of this thesis.

In Chapter 2 the effects of the atmosphere in optical wave propagation are introduced.

A novel formula for a general source beam is developed in Chapter 3 and the existing intensity profiles of many different types of source intensities are matched analytically with this novel formula.

Average received intensity of general beams in atmospheric turbulence is formulated in Chapter 4 and the variation of the average received intensities for various beam types are presented.

The thesis is finalized with the conclusion in chapter 5.

CHAPTER 2

EFFECTS OF THE ATMOSPHERE IN OPTICAL WAVE PROPAGATION

The atmosphere surrounds and protects the earth in the form of a gaseous blanket forming the transition between the solid surface of the earth and the near vacuum of the outer solar atmosphere. It acts as a shield against harmful radiation and meteors. The dynamics of the atmosphere drive the weather on the surface. It provides for life as part of the earth's biosphere. Optical propagation in this medium has many important characteristics and consequences. These reflect in applications such as meteorological remote sensing, infrared and visible astronomy, remote sensing and atmospheric optical communication systems. The atmosphere is composed of gases and suspended particles at various temperatures and pressures that vary as a function of altitude and azimuth. The variations in altitude show a marked structure. Six main horizontal layers [14] form the stratified structure of the atmosphere:

Troposphere: Contains roughly 75 % of the earth's atmospheric mass. Maximum air temperature occurs near the surface of the earth, but decreases with altitude to $-55^{\circ}C$.

Tropopause: It is an isothermal layer where air temperature remains constant at $-55^{\circ}C$.

Stratosphere: The air temperature in this layer increases with altitude because the ozone gas absorbs ultraviolet sunlight, thereby creating heat energy. The ozone layer, which protects life from harmful ultraviolet radiation, is concentrated between 10-15 km. Separating the mesosphere from the stratosphere is the stratopause, another isothermal layer.

Mesosphere: Temperature generally decreases at a constant rate down to $-90^{\circ}C$, the coldest in the atmosphere.

Mesopause: It is the third isothermal layer.

Thermosphere: Air temperature increases quite strongly above 90 km. This layer includes most of the ionosphere and the exosphere, the last being outermost region of the atmosphere [15].

In the atmosphere, low altitude laser transmissions are range and bit error limited by the atmospheric energy losses resulting from scattering during haze, rain, snow, and fog conditions in the atmospheric channel. Most atmospheric laser transmission wavelengths are generally chosen for their very low absorption losses, so that atomic or molecular energy transitions do not absorb free space laser energy [16].

2.1 Molecular and Aerosol Absorption

There are many types of gases in the atmosphere that can cause absorption. The dominant one is usually the water vapor in the wavelength region of interest for a Free Space Optics (FSO) system. By staying out of the “water” windows and keeping the path lengths short, absorption can largely be ignored. The two types of absorption are: Molecular absorption and aerosol absorption. Water vapor, CO_2 , NO_2 , CO and ozone are the primary radiation absorbers. Both CO_2 and water vapor are radiation absorbers at IR wavelengths.

2.2 Molecular and Aerosol Scattering

Scattering is a general physical process whereby some forms of radiation, such as light or moving particles, for example, are forced to deviate from a straight trajectory by one or more localized non-uniformities in the medium through which it passes. In conventional use, this also includes deviation of reflected radiation from the angle predicted by the law of reflection. Reflections that undergo

scattering are often called diffuse reflections and unscattered reflections are called specular (mirror-like) reflections.

There are two types of scattering mechanisms: Molecular (Rayleigh) and aerosol (Mie) scattering. Molecular scattering is significant for very long paths. It is caused by air molecules that are small in comparison with the wavelength λ of the radiation. The scattering coefficient is proportional to λ^{-4} , known as the Rayleigh law. For air molecules, scattering is negligible at $\lambda > 3 \mu\text{m}$. At $\lambda < 1 \mu\text{m}$, Rayleigh scattering produces the blue color of the sky because blue light is scattered much more than red light. Scattering by particles, or aerosol scattering, is different. This is especially true as the size of the particles approaches the wavelength of the transmitted light. The amount of scattering depends on the particle size distribution and the density of the particles. Wavelengths near the particle size are scattered very effectively (i.e. thick fogs or clouds look white) [17]. Scattering losses decrease rapidly with increasing wavelength, eventually approaching the Rayleigh scattering case. Mie scattering is the reason why sunsets appear red.

2.3 Free-Space Propagation of Gaussian-Beam Waves

Light propagates in the form of waves. In free space, light waves travel with a constant speed $c_0 = 3 \times 10^8$ m/s. The range of optical wavelengths contains three bands: Ultraviolet (10 to 390 nm), visible (390 to 760 nm) and infrared (760 nm to 1 mm) [18]. The corresponding range of optical frequencies stretches from 3×10^{11} Hz to 3×10^{16} Hz, as illustrated in Fig. (2-1).

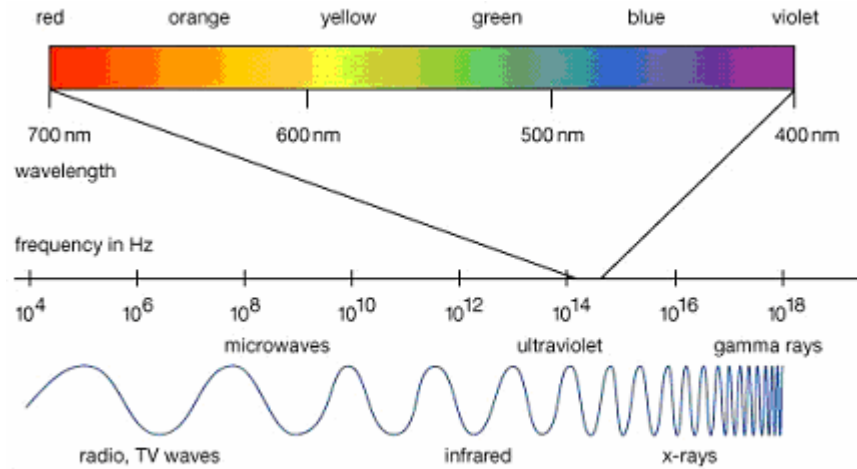


Figure 2-1 Electromagnetic Spectrum (www.yorku.ca).

There are several basic geometries commonly used to describe optical/IR wave models. These include the infinite plane wave, spherical wave, and Gaussian-beam wave.

An optical wave is described mathematically by a complex function of position $\vec{\mathbf{r}} = \vec{\mathbf{r}}(x, y, z)$ and time t , denoted by $u(\mathbf{r}, t)$ and known as the optical field. It satisfies the wave equation,

$$\nabla^2 u - \frac{1}{c^2} \frac{\partial^2 u}{\partial t^2} = 0, \quad (2.1)$$

where $c = \frac{c_0}{n}$ and n is the refractive index, ∇^2 is the Laplacian operator defined by

$$\nabla^2 = \frac{\partial^2}{\partial x^2} + \frac{\partial^2}{\partial y^2} + \frac{\partial^2}{\partial z^2}. \quad (2.2)$$

The optical intensity $I(\mathbf{r}, t)$ which is defined as the optical power per unit area (units of watts/cm²) is,

$$I(\mathbf{r}, t) = u(\mathbf{r}, t)u^*(\mathbf{r}, t), \quad (2.3)$$

where * denotes the complex conjugate.

The Gaussian-beam wave model used most often is the lowest order transverse electromagnetic (TEM) wave, denoted by TEM_{00} . Limiting cases of TEM_{00} Gaussian-beam wave leads to the infinite plane wave and spherical wave models.

The mathematical description of a propagating wave involves the notion of a field. In the case of electromagnetic radiation, the field may be a transverse electromagnetic (TEM) wave, whereas for acoustic waves the field may represent a pressure wave.

If we assume that time the variations in the field are sinusoidal, then we look for the solutions of Eq. (2.1) of the form $u(\mathbf{r}, t) = U_0(\mathbf{r})e^{-i\omega t}$, where ω is the angular frequency and $U_0(\mathbf{r})$ is the complex amplitude of the wave. The substitution of this solution form into Eq. (2.1) leads to the time independent reduced wave equation (or Helmholtz equation)

$$\nabla^2 U_0 + k^2 U_0 = 0, \quad (2.4)$$

where k is the optical wave number related to the optical wavelength λ by $k = \omega/c = 2\pi/\lambda$.

Most theoretical treatments of optical wave propagation have concentrated on simple models such as an unbounded plane wave or spherical wave, after that often taken as a point source. A plane wave is defined as one in which the equiphase surfaces (phase fronts) form parallel planes. The mathematical description of a general plane wave in the plane of the transmitter at on-axis is

$$U_0(x, y, 0) = A_0 e^{i\phi_0}, \quad (2.5)$$

where A_0 is a constant that represents the strength or amplitude of the wave field and ϕ_0 is the phase. If the plane wave is propagating along the positive z - axis in free space, the complex amplitude at distance z from the transmitter takes the approximate form

$$U_0(x, y, z) = A_0 e^{i\phi_0 + ikz}. \quad (2.6)$$

In the propagation of a lowest order Gaussian-beam wave, also called a TEM_{00} wave, with transmitting aperture located in the plane perpendicular to the propagation axis, it is assumed that the amplitude distribution in this plane is Gaussian with beam size, where $\sqrt{2}\alpha_s$ denotes the radius at which the field amplitude is e^{-1} of that on the beam axis shown in Fig. (2-2). It is assumed that the phase distribution is parabolic with radius of curvature F_0 . The cases $F_0 = \infty$, $F_0 > 0$, and $F_0 < 0$ correspond to collimated, convergent, and divergent beam forms.

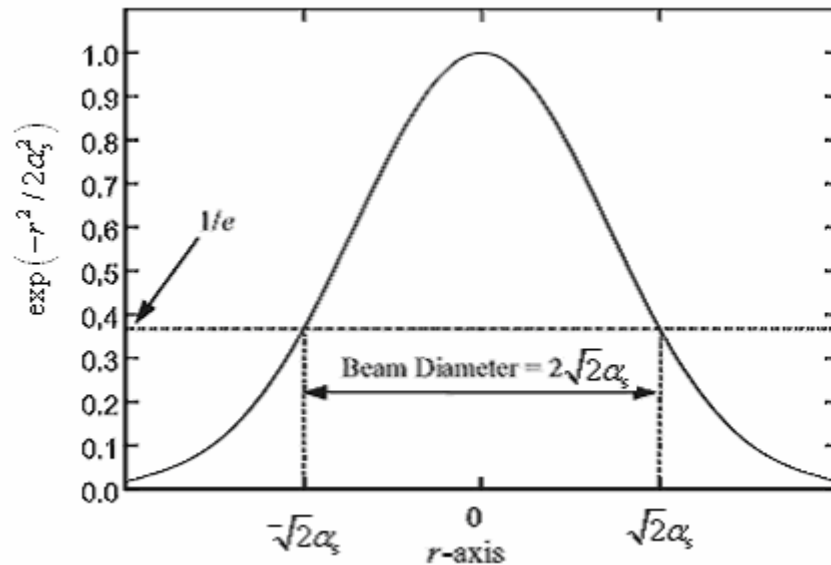


Figure 2-2 Amplitude profile of a Gaussian beam.

2.4 Atmospheric Turbulence and Extended Huygens-Fresnel Integral

2.4.1 Classical Turbulence and Kolmogorov Theory

Theoretical models of turbulence in the atmosphere were developed in the middle of the 20th-century particularly by Tatarski (1961), and were developed from much earlier studies of turbulence by Kolmogorov (1941). Their models assume that the turbulent power is initially generated on the largest scales and that dissipative forces cause the turbulent power to be transferred to smaller scales, eventually being dissipated on scales much smaller. These models make a good number of predictions about the characteristic length and timescales of the turbulence and in particular about the power spectrum of the fluctuations [19].

Naturally occurring small variations in temperature ($< 1^\circ C$) cause random changes in wind velocity, which can be viewed as turbulent motion in the atmosphere. The changes in temperature give rise to small changes in the atmospheric density and thus, to the index of refraction. These changes, on the order of 10^{-6} , can accumulate. The cumulative effect can cause significant inhomogeneities in the index profile of the atmosphere. This atmospheric turbulence can deteriorate the quality of the image formed at the receiver, and can cause fluctuations in the intensity and the phase of the received signal. Early studies by Kolmogorov suggest that a subclass of all optical turbulences has a degree of statistical consistency that permits a meaningful theoretical treatment. Optical turbulence is defined as the fluctuations in the index of refraction resulting from small temperature fluctuations. Random space-time redistribution of the refractive index causes a variety of effects on an optical wave related to its temporal irradiance fluctuations (scintillation) and phase fluctuations [20]. The wavefront of a beam will change in the course of propagation. This can lead to beam wander, intensity fluctuations (scintillations), and beam spreading [21].

These small changes in the refraction index act like small lenses in the atmosphere. They focus and redirect waves and eventually, through interference, cause intensity

variations. Each of these “lenses” has roughly the size of the turbulence eddy that caused it. The thin lens model is a useful approximation, but it is not completely accurate because there are no discontinuities in the atmosphere.

The most common effects of turbulence can be seen in the twinkling and quivering of stars. Twinkling is the random intensity variation of the light from a star because of the random interference between waves from the same star passing through slightly different atmospheric paths. The average position of the star also shows a random quiver because the average angle-of-arrival of light from the star is affected by the changing index of refraction along its path through the atmosphere. A third is the apparent spreading of the star image due to turbulence. The aberrations introduced by the optics did not account for the large spot image of the star, a point object [22].

Considering the atmosphere as a viscous fluid, experience has dictated that it has two distinct states of motion which are laminar and turbulent. The difference between these states lies in the fact that mixing does not occur in laminar flow for which the velocity flow characteristics are uniform or change in some regular fashion. In turbulent flow, the velocity field loses its uniform characteristics due to dynamic mixing and acquires random sub-flows called turbulent eddies.

In the earliest study of turbulent flow, Reynolds used similarity theory to define a non-dimensional quantity $Re = Vl/\nu$, the Reynolds number, V and l are the characteristic velocity and dimension of the flow. The transition from laminar flow to turbulent motion takes place at critical Reynolds number, above which the motion is considered turbulent.

Kolmogorov turbulence theory is the set of hypotheses that a small-scale structure is statistically homogeneous, isotropic, and independent of the large-scale structure. The source of energy at large scales is either wind shear or convection. When the wind velocity is sufficiently high that the critical Reynolds number is exceeded, large unstable air masses are created. Turbulent air motion represents a set of

vortices, or eddies, of various scale sizes, extending from a large scale size L_0 called the outer scale of turbulence to a microscale l_0 called the inner scale of turbulence. The outer scale L_0 represents the minimum distance over which the mean flow velocity changes by some appreciable amount. In the surface layer up to roughly 100 m the outer scale is assumed to grow linearly with the height of the observation point above ground. The inner scale is usually on the order of millimeters near the ground, but is generally thought to be on the order of centimeters in the upper atmosphere. Under the influence of inertial forces, large eddies break up into smaller ones, forming a continuous cascade of scale sizes between L_0 and l_0 known as the inertial range. Scale sizes smaller than the inner scale belong to the dissipation range.

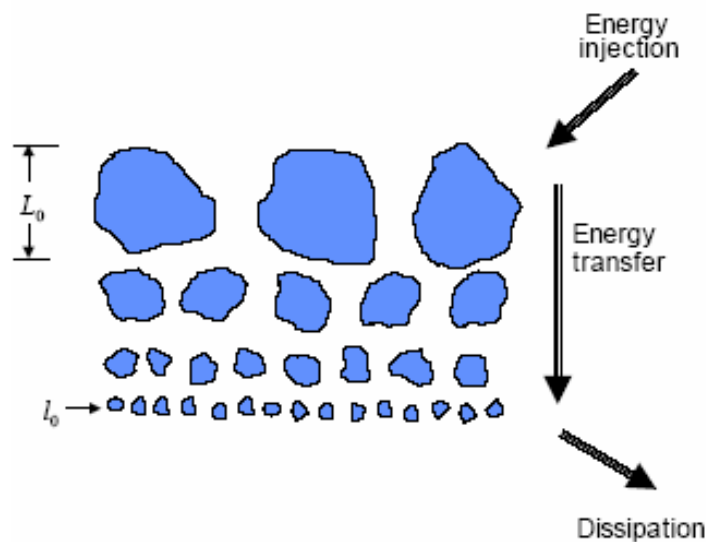


Figure 2-3 Kolmogorov cascade theory of turbulence, where L_0 denotes the outer scale and l_0 is the inner scale. Eddies between scale sizes l_0 and L_0 form the inertial subrange.

Classical turbulence generally refers to velocity fluctuations. However, turbulent fluctuations in wind speed result in the mixing of atmospheric quantities such as temperature, water vapor, and the refraction index. These quantities are called

passive scalars because their dynamics do not affect the turbulence associated with velocity fluctuations. The most important of these quantities in optical wave propagation are the index of refraction fluctuations which are commonly referred to as optical turbulence.

2.4.2 Laser Beam Propagation and the Extended Huygens-Fresnel Integral

The fundamental problem of optical wave propagation is the determination of the field at an observation point, given a disturbance specified over some finite aperture. In vacuum, the solution of this problem is given approximately by the Kirchoff integral, which is a mathematical expression of the Huygens-Fresnel principle. For this reason the Huygens-Fresnel principle can be extended to a medium that exhibits a variation in the refractive index [23].

In the laser beam propagation, we define $u(\mathbf{s}, 0) = u(s_x, s_y, 0)$ and $u(\mathbf{p}, L) = u(p_x, p_y, L)$ as the input and output fields of a linear system. In the atmosphere, the field changes with the distance L . The field at the receiver can be expressed as :

$$u(p_x, p_y, L) = G(\mathbf{s}, \mathbf{p}; L) \otimes u(s_x, s_y, 0), \quad (2.7)$$

where \otimes is the convolution operator and $G(\mathbf{s}, \mathbf{p}; L)$ is the Green's function [24] defined

$$G(\mathbf{s}, \mathbf{p}; L) = \frac{1}{4\pi L} \exp\left[ikL + \frac{ik}{2L} |\mathbf{s} - \mathbf{p}|^2 \right] \exp[\psi(\mathbf{s}, \mathbf{p})]. \quad (2.8)$$

Here $\psi(\mathbf{s}, \mathbf{p})$ is the random part of the complex phase of a spherical wave propagating in the turbulent medium from the point $(\mathbf{s}, 0)$ to the point (\mathbf{p}, L) .

In this more general formulation the complex amplitude at propagation distance L from the source is represented by the extended Huygens-Fresnel integral as

$$u(\mathbf{p}, L) = -2ik \int_{-\infty}^{\infty} \int_{-\infty}^{\infty} G(\mathbf{s}, \mathbf{p}; L) u(\mathbf{s}, 0) d^2\mathbf{s}, \quad (2.9)$$

$$u(\mathbf{p}, L) = \frac{-ik}{2\pi L} \exp(ikL) \int_{-\infty}^{\infty} \int_{-\infty}^{\infty} u(\mathbf{s}, 0) \exp\left[\frac{ik}{2L} |\mathbf{s} - \mathbf{p}|^2\right] \exp[\psi(\mathbf{s}, \mathbf{p})] d^2\mathbf{s}. \quad (2.10)$$

CHAPTER 3

FORMULATION OF GENERAL SOURCE BEAM AND THE LIMITING CASE RESULTS

In this section the existing optical beam fields such as Bessel, Bessel Gaussian, Laguerre, Laguerre Gaussian, Ince Gaussian, dark hollow, bottle, super Gaussian, Lorentz, flat-topped, Hermite-sinusoidal-Gaussian, sinusoidal-Gaussian such as cos-Gaussian, sine-Gaussian, cosh-Gaussian, sinh-Gaussian, annular and their higher order modes with their truncated, elegant and elliptical versions are combined in a single general source beam formulation.

A general source beam equation can be generated from all the mentioned beams' source equations. In this part, all the mentioned beams' source equations are investigated and huddled together to obtain Eq. (3.1). After collecting these source fields in a general formula and writing it in a compact form, a general source beam wave field at the source plane ($z = 0$) will have an electric field distribution of

$$\begin{aligned}
 u(s_x, s_y, 0) = & \sum_{\ell=1}^N A_{\ell} T_{\ell} \frac{\left[P(s_x^2 + s_y^2)^{\gamma_1} + R(s_x^2 + s_y^2)^{\gamma_2} \right]^{\gamma_3}}{\left(d_1 \alpha_{sx\ell}^2 + s_x^2 \right)^{c_1} \left(d_2 \alpha_{sy\ell}^2 + s_y^2 \right)^{c_2}} \\
 & \times (A - V) \cos(Y) \exp \left[-j \left(V_{x\ell} s_x + V_{y\ell} s_y \right) \right] \\
 & \times H_n \left(a_{x\ell} s_x + b_{x\ell} \right) H_m \left(a_{y\ell} s_y + b_{y\ell} \right), \quad (3.1)
 \end{aligned}$$

s_x and s_y are the x and y components of the source plane vector \mathbf{s} , i.e., $\mathbf{s} = (s_x, s_y)$. All ℓ subscripted terms establish the specific parameters of the individual beams comprising the general beam through summation. In this manner,

N denotes the number of beams, A_ℓ is the complex amplitude of the field at the origin of the source plane, θ_ℓ is the phase, $H_n(a_{x\ell}s_x + b_{x\ell})$ and $H_m(a_{y\ell}s_y + b_{y\ell})$ are Hermite polynomials governing the beam variations for s_x and s_y directions, where n and m are the order, $a_{x\ell}$ and $a_{y\ell}$ characterize the width, $b_{x\ell}$ and $b_{y\ell}$ are the complex displacement parameters, $V_{x\ell}$, $V_{y\ell}$ are the complex parameters, used to create physical location displacement and phase rotation or a combination of both, named as the displacement parameters, $\alpha_{sx\ell}$ and $\alpha_{sy\ell}$ are the source sizes, k is the wave number,

$$V = \left[B - C \exp \left(-D \left(\frac{s_x}{(\alpha_{sx\ell})^{f_1}} \right)^{F_1} - E \left(\frac{s_y}{(\alpha_{sy\ell})^{f_2}} \right)^{F_2} \right) - G \exp \left(-H \left(\frac{s_x}{\alpha_{sx\ell}} \right)^{F_4} - J \left(\frac{s_y}{\alpha_{sy\ell}} \right)^{F_5} - jm_2\phi \right) \right]^{F_3}, \quad (3.2)$$

$$Y = \left(m_{i,j} \cosh^{-1} \left[\sqrt{\frac{(f^2 + |s|^2) \pm \sqrt{(f^2 + |s|^2)^2 - 4f^2s_x^2}}{2f^2}} \right] - m_i \sin^{-1} \left[\sqrt{\frac{(f^2 - |s|^2) \pm \sqrt{(|s|^2 - f^2)^2 + 4f^2s_y^2}}{2f^2}} \right] \right), \quad (3.3)$$

ϕ is the phase factor, f is the semi focal parameter and other parameters such as T_r , P , R , γ_1 , γ_2 , γ_3 , d_1 , d_2 , c_1 , c_2 , A , B , C , D , E , M , G , H , J , F_1 , F_2 , F_3 , F_4 , F_5 , F_6 , f_1 , f_2 , m_i are the variable parameters which change with the limiting conditions in order to obtain the reduced forms of the beam.

The intensity of the optical wave is the squared magnitude of the field. Thus, at the source plane, the intensity is

$$I(\mathbf{s}, 0) = |u(\mathbf{s}, 0)|^2, \quad (3.4)$$

where $u(\mathbf{s}, 0) = u(s_x, s_y, 0)$. The intensity distribution of the general beam at the exit plane of the laser can be calculated by using Eq. (3.4) for all the cases.

3.1 Limiting Cases

From the general source beam formulation given by Eq. (3.1), the above mentioned beams' source equations can be obtained in the limiting cases. Also the mentioned beams' intensities can be calculated by using Eq. (3.1) and Eq. (3.4). Here Eq. (3.1) is checked and found to reduce to the following limiting cases correctly.

3.1.1 Bessel Beam

Bessel beams are non-diffracting beams, that is as they propagate they do not spread out. If we focus a normal laser beam down to a small spot we find that it spreads out very quickly, indeed the smaller the spot the more quickly it spreads. There are solutions to the (Helmholtz) wave equation which describe beams that do not spread out in this way and one family of these beams is called Bessel beams, as they are mathematically described by Bessel functions. Bessel functions of the first kind [25] is defined as

$$J_n(s_x) = \sum_{\tau=0}^{\infty} \frac{(-1)^\tau (s_x/2)^{2\tau+n}}{\tau!(\tau+n)!}, \quad (3.5)$$

where n is the order of Bessel function. Defining the relevant parameters in Eq. (3.1) as

$$\begin{aligned} \ell = \xi + 1, \quad N \rightarrow \infty, \quad A_\ell = \frac{E_0 \left(-\frac{\pi^2}{\lambda^2} \sin^2 \theta \right)^\xi}{\zeta! \Gamma(\zeta + 1)}, \quad T_r = 1, \quad P = 1, \\ \gamma_1 = \xi, \quad R = 0, \quad \gamma_3 = 1, \quad c_1 = 0, \quad c_2 = 0, \quad A = 2, \quad F_3 = 0, \quad m_i = 0, \\ n = 0, \quad m = 0, \quad V_{x\ell} = 0, \quad V_{y\ell} = 0, \end{aligned} \quad (3.6)$$

Bessel beam can be obtained. Substituting the parameter set in Eq. (3.6) into Eq. (3.1), Eq. (3.2) and Eq. (3.3), Bessel beam source equation is obtained [26]. After

substitution, the reduced form of the general source beam equation can be written as

$$u(s_x, s_y, 0) = \sum_{\zeta=0}^{\infty} E_0 (s_x^2 + s_y^2)^{\zeta} \times \frac{\left(-\frac{\pi^2}{\lambda^2} \sin^2 \theta\right)^{\zeta}}{\zeta! \Gamma(\zeta + 1)}, \quad (3.7)$$

where E_0 is a constant, λ being the wavelength and $\Gamma(n)$ is the gamma function, where $\Gamma(n) = (n-1)!$.

Substituting Eq. (3.1), Eq. (3.2) and Eq. (3.3) into Eq. (3.4), Bessel intensity at source plane is calculated using the general source beam formulation. Fig. (3-1) shows the Bessel beam intensity at the source plane.

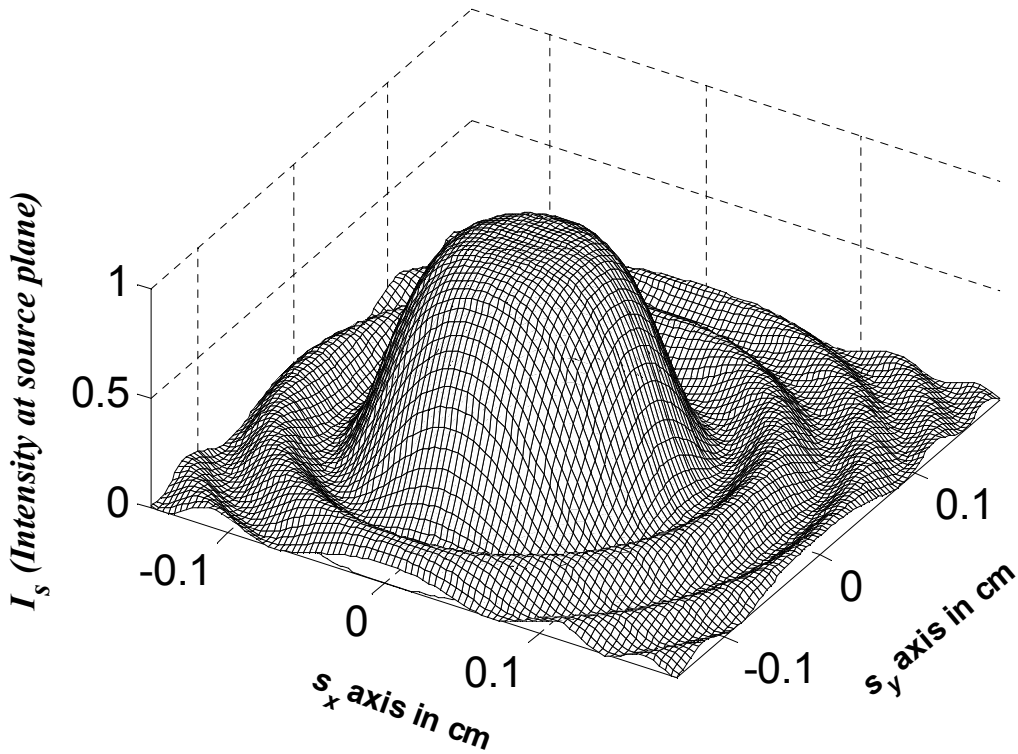


Figure 3-1 Intensity distribution of Bessel beam the source plane.

3.1.2 Bessel Gaussian Beam

Bessel Gaussian beam is found by multiplying Bessel beam equation by the Gaussian expression which can be defined as

$$u(s_x, s_y, 0) = E_0 \exp\left(-\frac{s_x^2}{2\alpha_{sx}^2} - \frac{s_y^2}{2\alpha_{sy}^2}\right), \quad (3.8)$$

where E_0 is a constant that represents the amplitude. Multiplying Eq. (3.7) by Eq. (3.8), Bessel Gaussian source equation can be obtained. Defining the relevant parameters in Eq. (3.1) as

$$\begin{aligned} \ell &= \zeta + 1, \quad N \rightarrow \infty, \quad A_\ell = \frac{\left(-\frac{\pi^2}{\lambda^2} \sin^2 \theta\right)^\zeta}{\zeta! \Gamma(\zeta + 1)}, \quad T_r = 1, \quad P = 1, \quad \gamma_1 = \zeta, \\ R &= 0, \quad \gamma_3 = 1, \quad c_1 = 0, \quad c_2 = 0, \quad A = 0, \quad B = 0, \quad C = -1, \quad D = \frac{1}{2}, \quad F_1 = 2, \\ E &= \frac{1}{2}, \quad F_2 = 2, \quad G = 0, \quad F_3 = 1, \quad m_i = 0, \quad n = 0, \quad m = 0, \quad V_{x\ell} = 0, \\ V_{y\ell} &= 0, \quad f_1 = 1, \quad f_2 = 1, \end{aligned} \quad (3.9)$$

Bessel Gaussian beam is obtained. Substituting Eq. (3.9) into Eq. (3.1), Eq. (3.2) and Eq. (3.3), the general source beam equation reduces to the Bessel Gaussian source equation [27] as

$$\begin{aligned} u(s_x, s_y, 0) &= \sum_{\zeta=0}^{\infty} E_0 (s_x^2 + s_y^2)^\zeta \frac{\left(-\frac{\pi^2}{\lambda^2} \sin^2 \theta\right)^\zeta}{\zeta! \Gamma(\zeta + 1)} \\ &\times \exp\left(-\frac{s_x^2}{2\alpha_{sx}^2} - \frac{s_y^2}{2\alpha_{sy}^2}\right), \end{aligned} \quad (3.10)$$

which is a Bessel Gaussian source equation. Eq. (3.10) is the multiplication of Eq. (3.7) and Eq. (3.8). Also the intensity can be calculated by using Eq. (3.4).

3.1.3 Laguerre Beam

The Laguerre beam modes are approximate solutions to the wave equation in cylindrical coordinates, which are valid when the wave propagates in nearly parallel beams. The beam-mode superposition representing the transverse electric field E of an axially-symmetric beam, in cylindrical polar coordinates (r, ϕ, z) , with the z -axis being coincident with the beam axis, where $r = \sqrt{s_x^2 + s_y^2}$. Laguerre source field equation can be defined as [28]

$$u_{mn}(r, \phi, 0) = \left(\frac{\sqrt{2}r}{W_0} \right) L_n^m \left(\frac{2r^2}{W_0^2} \right) \exp(-jm\phi), \quad (3.11)$$

where $L_n^m(x)$ is the associated Laguerre function which can be described as

$$L_n^m(x) = \sum_{\tau=0}^n (-1)^\tau \frac{(n+m)!}{(n-\tau)!(m+\tau)!\tau!} x^\tau, \quad (3.12)$$

and W_0 is the width of the beam waist. Defining the relevant parameters in Eq. (3.1) as

$$\begin{aligned} \ell = \zeta + 1, \quad A_\ell &= \frac{(-1)^\zeta (N + m_3)!}{(\alpha_{sx}^{m_3+2\zeta} + \alpha_{sy}^{m_3+2\zeta})(N - \zeta)!(m_3 + \zeta)!\zeta!}, \\ T_r = 1, \quad P = 1, \quad R = 0, \quad \gamma_1 &= \zeta + \frac{m_3}{2}, \quad \gamma_3 = 1, \quad c_1 = 0, \quad c_2 = 0, \quad A = 0, \\ B = 0, \quad C = 0, \quad G = -1, \quad H = 0, \quad J = 0, \quad m_2 = m_3, \quad m_i = 0, \quad V_{x\ell} &= 0, \\ V_{y\ell} = 0, \quad n = 0, \quad m = 0, \end{aligned} \quad (3.13)$$

Laguerre beam is obtained. After substituting Eq. (3.13) into Eq. (3.1), Eq. (3.2) and Eq. (3.3), the reduced form of Eq. (3.1) can be written as

$$\begin{aligned}
u_{m_3 n_3}(r, \phi, 0) = & \sum_{\zeta=0}^N \frac{(-1)^\zeta (s_x^2 + s_y^2)^{\zeta+m_3/2} (N+m_3)! 2^{\zeta+\left(\frac{m_3-1}{2}\right)}}{(\alpha_{sx}^{m_3+2\zeta} + \alpha_{sy}^{m_3+2\zeta})(N-\zeta)!(m_3+\zeta)!\zeta!} \\
& \times \exp(-jm_3\phi), \tag{3.14}
\end{aligned}$$

which is a Laguerre source beam equation [28], where N and m_3 are mode numbers of the Laguerre polynomial.

3.1.4 Laguerre Gaussian Beam

Multiplying Eq. (3.11) by the Gaussian expression, Laguerre Gaussian source beam equation is obtained. Defining the relevant parameters in Eq. (3.1) as

$$\begin{aligned}
\ell = \zeta + 1, \quad A_\ell = & \frac{(-1)^\zeta (N+m_3)!}{(\alpha_{sx}^{m_3+2\zeta} + \alpha_{sy}^{m_3+2\zeta})(N-\zeta)!(m_3+\zeta)!\zeta!}, \\
T_r = 1, \quad P = 1, \quad R = 0, \quad \gamma_1 = & \xi + \frac{m_3}{2}, \quad \gamma_3 = 1, \quad c_1 = 0, \quad c_2 = 0, \quad A = 0, \quad B = 0, \\
C = 0, \quad G = -1, \quad H = 0.5, \quad J = 0.5, \quad m_2 = & m_3, \quad m_i = 0, \quad F_4 = 2, \quad F_5 = 2, \\
F_3 = 1, \quad V_{x\ell} = 0, \quad V_{y\ell} = 0, \quad n = 0, \quad m = & 0, \tag{3.15}
\end{aligned}$$

Laguerre Gaussian beam is obtained. After substituting Eq. (3.15) into Eq. (3.1), Eq (3.2) and Eq. (3.3), the general source beam formulation reduces to

$$\begin{aligned}
u_{N_3}^{m_3}(s_x, s_y, 0) = & \sum_{\zeta=0}^N \frac{(-1)^\zeta (s_x^2 + s_y^2)^{\zeta+m_3/2} (N+m_3)!}{(\alpha_{sx}^{m_3+2\zeta} + \alpha_{sy}^{m_3+2\zeta})(N-\zeta)!(m_3+\zeta)!\zeta!} \\
& \times \exp\left(-\frac{s_x^2}{2\alpha_{sx}^2} - \frac{s_y^2}{2\alpha_{sy}^2} - jm_3\phi\right), \tag{3.16}
\end{aligned}$$

which is the Laguerre Gaussian source field equation [28].

The Laguerre Gaussian beam (0,1) reduces to the Hermite Gaussian beam (1,0) which can be seen in Fig. (3-2).

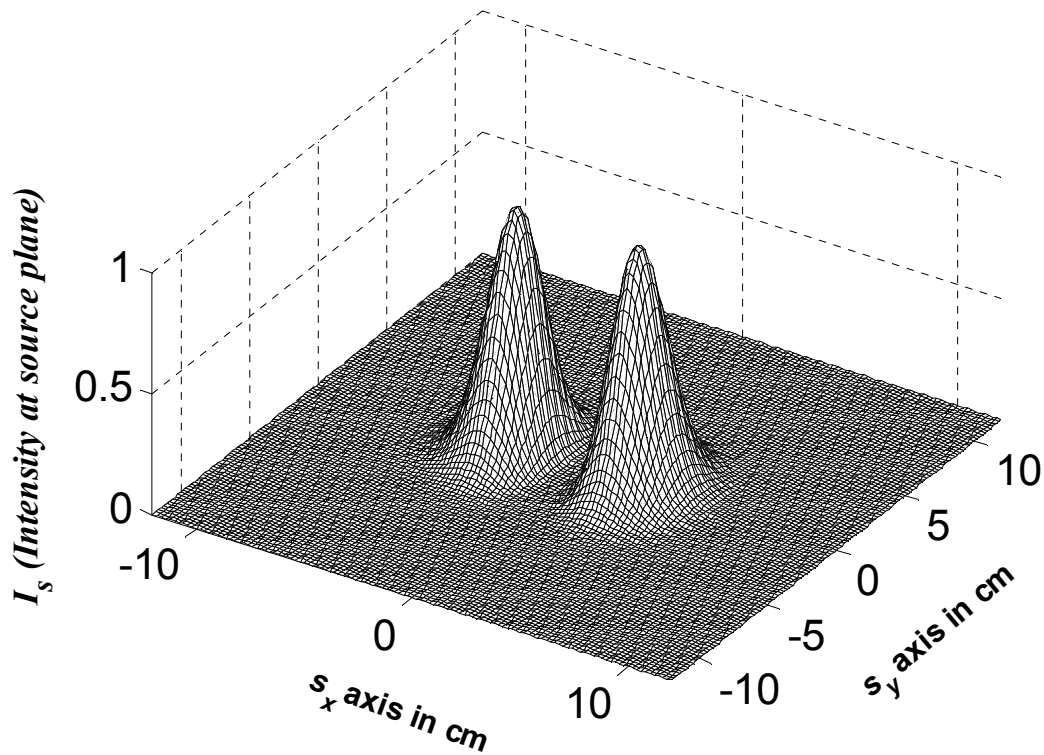


Figure 3-2 Intensity distribution of Laguerre Gaussian beam at the source plane with mode orders (0,1).

3.1.5 Ince Gaussian Beam

Ince Gaussian modes form a complete family of exact and orthogonal solutions of the paraxial wave equation for elliptical coordinates. The transverse distribution of these fields is described by the Ince polynomials and have an inherent elliptical symmetry. These modes constitute a smooth transition from Hermite Gaussian modes to Laguerre Gaussian modes. Any paraxial field can be obtained by linear superposition of Ince Gaussian beams with the appropriate weighting and phase factors. To obtain solutions of the paraxial wave equation in elliptical coordinates a

wave is considered whose complex envelope is a modulated version of the Gaussian beam,

$$u(r, \phi, 0) = E(\xi) N(\eta) \exp\left(-\frac{s_x^2}{2\alpha_{sx}^2} - \frac{s_y^2}{2\alpha_{sy}^2}\right), \quad (3.17)$$

with

$$\frac{d^2 E}{d\xi^2} - \epsilon \sinh 2\xi \frac{dE}{d\xi} = (\mu - p \epsilon \cosh 2\xi) E, \quad (3.18)$$

$$\frac{d^2 N}{d\eta^2} + \epsilon \sin 2\eta \frac{dN}{d\eta} = -(\mu - p \epsilon \cos 2\eta) N, \quad (3.19)$$

$r = \sqrt{s_x^2 + s_y^2}$, E and N are real functions, ξ and η are the complex elliptical radial and angular variables, p and η are separation constants, ϵ is the ellipticity parameter of the Ince Gaussian eigenmode which is $\epsilon = 2f^2 / W^2$. Eq. (3.17) satisfies the paraxial wave equation in elliptical coordinates so it can be solved by using Eq. (3.18) and Eq. (3.19).

Defining the relevant parameters in Eq. (3.1) as

$$\begin{aligned} N = 1, A_\ell = 1, T_r = 1, \gamma_3 = 0, c_1 = 0, c_2 = 0, A = 0, B = 0, \\ C = -1, D = \frac{1}{2}, G = 0, E = \frac{1}{2}, V_{x\ell} = 0, V_{y\ell} = 0, n = 0, \\ m = 0, F_1 = 2, F_2 = 2, F_3 = 1, m_i = m, f_1 = 1, f_2 = 1, \end{aligned} \quad (3.20)$$

Ince Gaussian beam is obtained. After substituting Eq. (3.20) into Eq. (3.1), Eq. (3.2) and Eq. (3.3), the source field equation of Ince Gaussian beam [29] is obtained. After the substitution, the reduced form of Eq. (3.1) can be obtained as

$$u(r, \phi, 0) = \exp\left(-\frac{s_x^2}{2\alpha_{sx}^2} - \frac{s_y^2}{2\alpha_{sy}^2}\right) \cos(Y), \quad (3.21)$$

where

$$Y = m_i j \cosh^{-1} \left(\sqrt{\frac{(f^2 + |s|^2) \pm \sqrt{(f^2 + |s|^2)^2 - 4f^2 s_x^2}}{2f^2}} \right) - m_i \sin^{-1} \left(\sqrt{\frac{(f^2 - |s|^2) \pm \sqrt{(|s|^2 - f^2)^2 + 4f^2 s_y^2}}{2f^2}} \right). \quad (3.22)$$

Here, $0 \leq m_i \leq p$ for even functions and $1 \leq m_i \leq p$ for odd functions. Eq. (3.21) is the reduced form of the Eq. (3.1) after substitution.

3.1.6 Dark Hollow Beam

Optical beams with zero central intensity are called dark hollow beams. A dark hollow beam can be expressed as a finite sum of Laguerre Gaussian beams or Gaussian beams [30]. Dark hollow beam is a special case of higher-order annular beams which will be mentioned later. A higher-order annular beam source is defined as the superposition of two different higher-order Hermite Gaussian beams. A special case of such an excitation is the annular Gaussian beam in which two beams operate at fundamental modes of different Gaussian beam sizes, yielding a doughnut-shaped (annular) beam when the second beam is subtracted from the first beam.

The electric field of a dark hollow beam at $z = 0$ can be expressed as the following finite sum of Gaussian beams

$$u(s_x, s_y, 0) = \sum_{n=1}^N \frac{(-1)^{n-1}}{N} \binom{N}{n} \times \left[\exp\left(-\frac{ns_x^2 + ns_y^2}{W_0^2}\right) - \exp\left(-p \frac{ns_x^2 + ns_y^2}{W_0^2}\right) \right], \quad (3.23)$$

where $\binom{N}{n}$ denotes a binomial coefficient, N is the order of a circular dark hollow

beam, W_0 determines the beam waist width, and $p = \frac{1}{\varepsilon^2}$ with $p < 1$.

Defining the relevant parameters in Eq. (3.1) as

$$\begin{aligned} \ell &= \xi, \quad A_\ell = \frac{(-1)^{\xi-1}}{N} \frac{N!}{\xi!(N-\xi)!}, \quad T_r = 1, \quad \gamma_3 = 0, \\ c_1 &= 0, \quad c_2 = 0, \quad A = 0, \quad B = 0, \quad C = -1, \quad D = \frac{\xi}{2}, \quad G = 0, \quad m_i = 0, \\ E &= \frac{\xi}{2\varepsilon^2}, \quad F_1 = 2, \quad F_2 = 2, \quad F_3 = 1, \quad f_1 = 1, \quad f_2 = 1, \quad V_{xl} = 0, \quad V_{yl} = 0, \\ n &= 0, \quad m = 0, \end{aligned} \quad (3.24)$$

dark hollow beam is obtained. After substituting Eq. (3.24) into Eq. (3.1), Eq. (3.2) and Eq. (3.3), the general source beam equation reduces to

$$u(s_x, s_y, 0) = \sum_{\zeta=1}^N \frac{(-1)^{\zeta-1}}{N} \frac{N!}{\zeta!(N-\zeta)!} \times \left[\exp\left(-\frac{\zeta(s_x^2 + s_y^2)}{2(\alpha_{sx}^2 + \alpha_{sy}^2)}\right) - \exp\left(-\frac{\zeta(s_x^2 + s_y^2)}{2\varepsilon^2(\alpha_{sx}^2 + \alpha_{sy}^2)}\right) \right], \quad (3.25)$$

which is dark hollow source beam equation [30]. Eq. (3.25) is the dark hollow beam source equation, where $\varepsilon < 1$ and N_4 is the order of a circular dark hollow beam. Using Eq. (3.4) the intensity at source plane can be calculated. Fig. (3-3) shows the intensity distribution plot of dark hollow beam at the source plane.

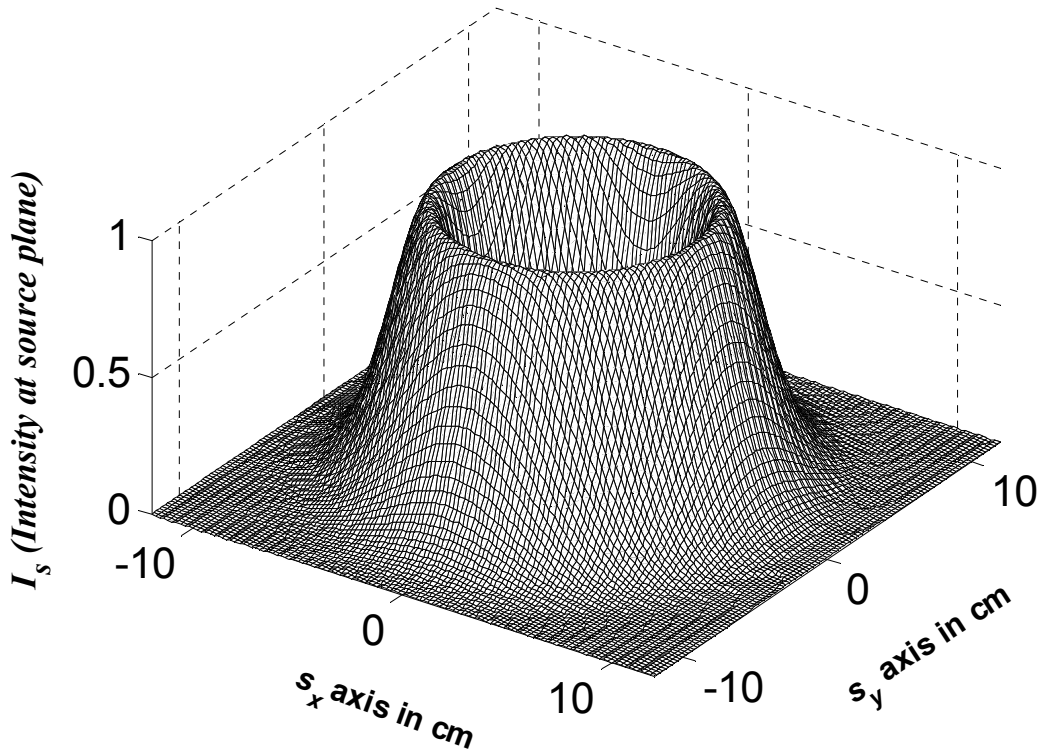


Figure 3-3 Intensity distribution of dark hollow beam at the source plane.

3.1.7 Bottle Beam

The optical bottle beam may be considered to be a superposition of two or more coaxial and confocal Laguerre Gaussian beams that are adjusted so as to interfere destructively at center of the focal plane. At this position, the dissimilar radial dependences of the Laguerre Gaussian beams cause exact cancellation to be lost off axis, and different Gouy phases play similar role away from the focal plane. This representation was proposed by Arlt and Padgett [31], who used a holographic mode converter to form a simple bottle beam superposition of $L(0,0)$ and $L(2,0)$. The electric field of the bottle beam can be defined as

$$E(r, \phi, 0) = L_{00}(r, 0) - L_{20}(r, 0), \quad (3.26)$$

where L_{00} and L_{20} are the Laguerre polynomials and $L_{00} = L(0,0)$, $L_{20} = L(2,0)$.

Defining the relevant parameters in Eq. (3.1) as

$$\begin{aligned}
N &= 1, A_\ell = 1, T_r = 1, c_1 = 0, c_2 = 0, P = \frac{-1}{2\alpha_{sx}^4}, \gamma_1 = 2, \\
R &= \frac{2}{\alpha_{sy}^2}, \gamma_2 = 1, \gamma_3 = 1, A = 0, B = 0, C = -1, D = \frac{1}{2}, \\
E &= \frac{1}{2}, G = 0, f_1 = 1, f_2 = 1, F_1 = 2, F_2 = 2, F_3 = 1, \\
V_{x\ell} &= 0, V_{y\ell} = 0, n = 0, m = 0,
\end{aligned} \tag{3.27}$$

bottle beam is obtained. Substituting Eq. (3.27) into Eq. (3.1), Eq. (3.2) and Eq. (3.3), reduced form of the general source beam equation is

$$\begin{aligned}
E(r, 0) &= L_{00}(r, z) - L_{20}(r, z) \\
&= \exp\left(-\frac{1}{2}\left(\frac{s_x^2}{\alpha_{sx}^2} + \frac{s_y^2}{\alpha_{sy}^2}\right)\right) \\
&\quad \times \left\{ \frac{-(s_x^2 + s_y^2)^2}{2\alpha_{sx}^4} + \frac{2(s_x^2 + s_y^2)}{\alpha_{sy}^2} \right\},
\end{aligned} \tag{3.28}$$

which satisfies bottle beam source equation [32]. With general source beam formulation, the intensity can be calculated by using Eq. (3.4). Fig. (3-4) shows the intensity distribution at the source plane.

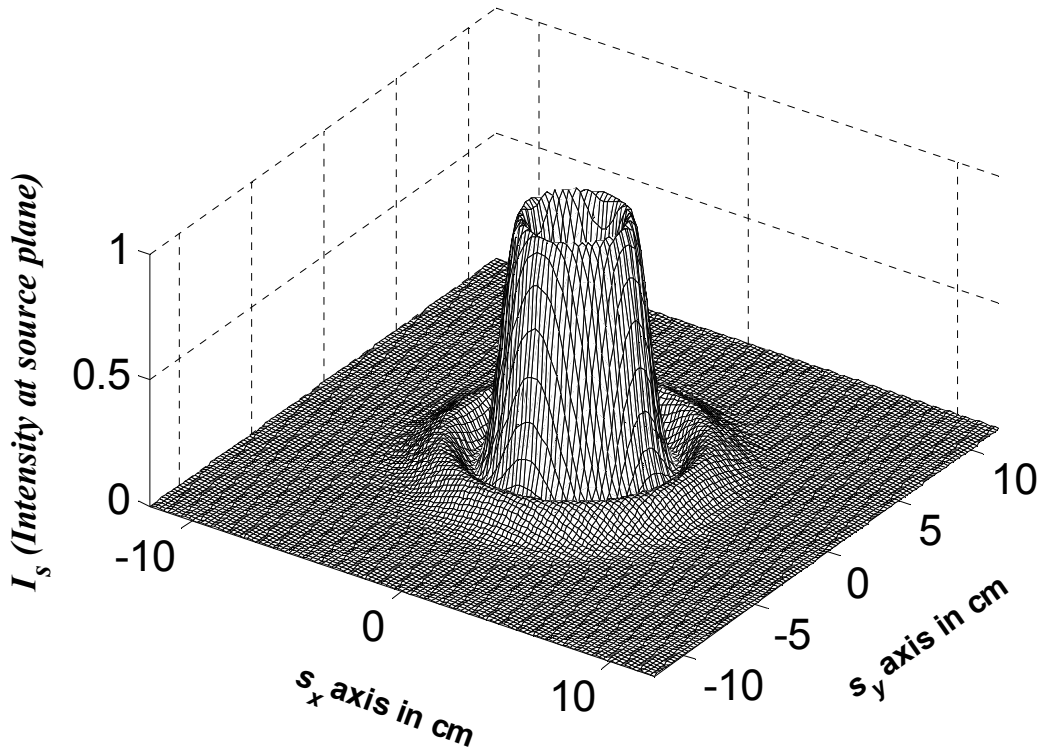


Figure 3-4 Bottle beam intensity at the source plane.

3.1.8 Flat-topped Beam

To avoid diffraction effects in regions of sharp changes in the intensity after beam shaping, several analytic functions with a uniform central region and a continuous variation from the uniform region to the almost null region have been studied and reported in the literature. In past years, several models have been proposed to describe light beams with flat-topped profiles [33]. The super Gaussian beam is one of the models that matches such requirements. Flattened Gaussian beam can be expressed as a sum of finite Laguerre Gaussian modes or Hermite Gaussian modes.

Flat-topped beam source equation can be defined as

$$u_s(s_x, s_y, 0) = 1 - \left[1 - \exp\left(-s_x^2 / \alpha_{sx}^2 - s_y^2 / \alpha_{sy}^2\right) \right]^{N_f}, \quad (3.29)$$

where N_f is the order parameter for flatness, such that $N_f = 1$. When $N_f \neq 1$, on the other hand, the beam sizes will depart from Gaussian source sizes along s_x and s_y directions.

Defining the relevant parameters in Eq. (3.1) as

$$\begin{aligned}
 N &= 1, A_\ell = 1, T_r = 1, A = 1, B = 1, C = 1, D = 1, \\
 E &= 1, F_1 = 2, F_2 = 2, F_3 = N_f, f_1 = 1, f_2 = 1, \\
 G &= 0, m_i = 0, V_{x\ell} = 0, V_{y\ell} = 0, n = 0, m = 0,
 \end{aligned} \tag{3.30}$$

flat-topped beam is obtained. Substituting Eq. (3.30) into Eq. (3.1), Eq. (3.2) and Eq. (3.3), the general source beam formulation reduces to a flat-topped beam source equation [33]. The intensity can be calculated using Eq. (3.4). Fig. (3-5) is the intensity plot for flat-topped beam at the source plane when $N_f = 10$.

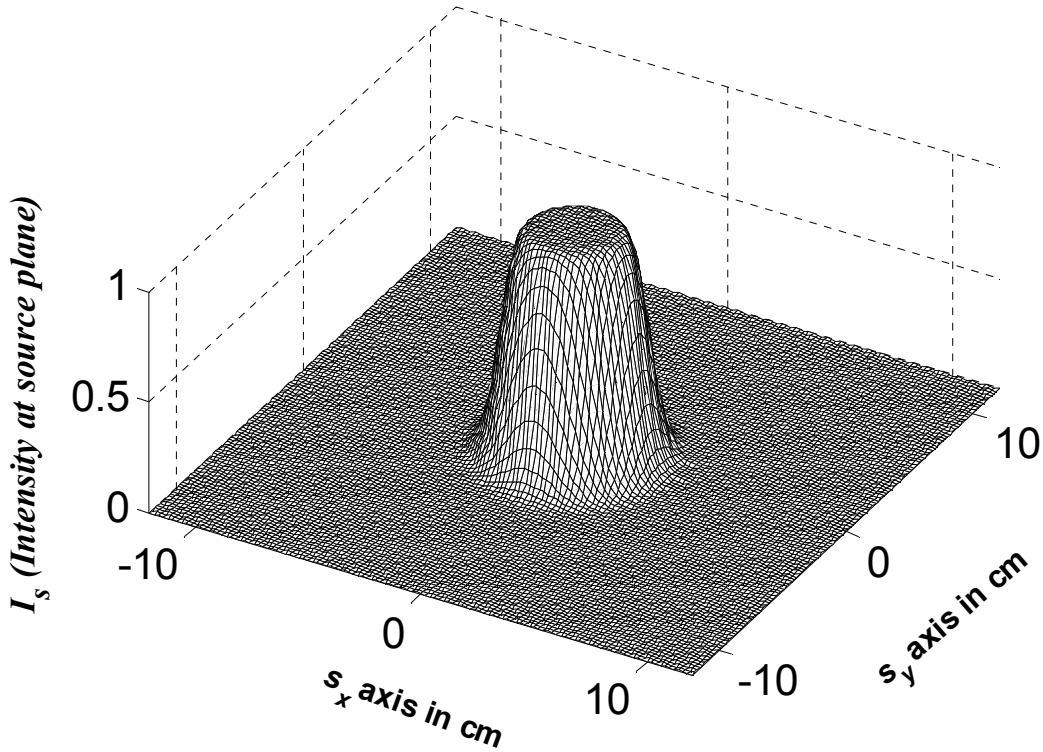


Figure 3-5 Flat-topped intensity at the source plane with $N_f = 10$.

3.1.9 Super Gaussian Beam

One of the most popular models for describing flat-topped profiles is the super Gaussian function [34],

$$u(s_x, s_y, 0) = \exp \left[- \left(\frac{s_x}{\sqrt{2}\alpha_{sx}} \right)^{N_s} - \left(\frac{s_y}{\sqrt{2}\alpha_{sy}} \right)^{N_s} \right], \quad (3.31)$$

where N_s is the super Gaussian power. Usually, N_s is an even integer and Eq. (3.31) reduces to the Gaussian case when $N_s = 2$.

Defining the relevant parameters in Eq. (3.1) as

$$\begin{aligned} N &= 1, T_r = 1, A_\ell = 1, \gamma_3 = 0, c_1 = 0, c_2 = 0, A = 0, B = 0, C = -1, \\ D &= \frac{1}{(\sqrt{2})^{N_s}}, E = \frac{1}{(\sqrt{2})^{N_s}}, G = 0, F_1 = N_s, F_2 = N_s, F_3 = 1, mi = 0, \\ V_{x\ell} &= 0, V_{y\ell} = 0, n = 0, m = 0, f_1 = 1, f_2 = 1, \end{aligned} \quad (3.32)$$

super Gaussian beam is obtained. After substituting Eq. (3.32) into Eq. (3.1), Eq. (3.2) and Eq. (3.3), the general source beam formulation reduces to a super Gaussian beam source equation [34]. Fig. (3-6) shows the intensity plot for $N_s = 8$ at the source plane.

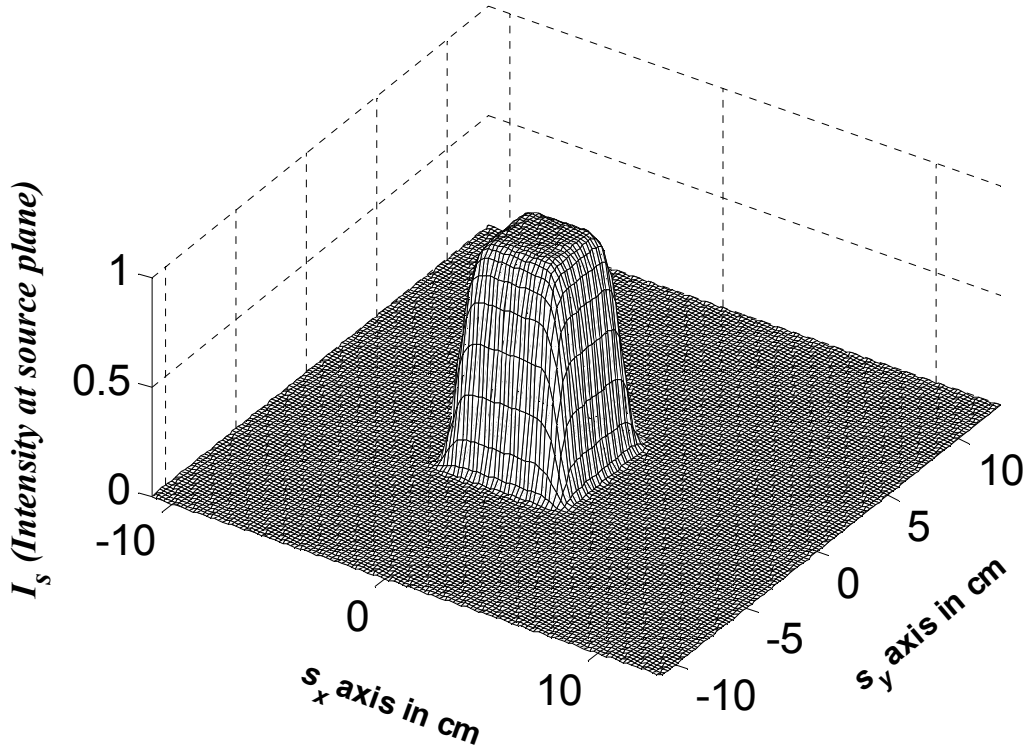


Figure 3-6 Super Gaussian beam intensity at the source plane for $N_s = 8$.

3.1.10 Lorentz Beam

These beams are called Lorentz beams because the form of their transverse pattern in the source plane is the product of two independent Lorentz functions [35]. Lorentz beam source equation can be defined as

$$u(s_x, s_y, 0) = \frac{E_0}{W_x W_y} \frac{1}{\left[1 + (s_x / W_x)^2\right]} \frac{1}{\left[1 + (s_y / W_y)^2\right]}, \quad (3.33)$$

where E_0 is a constant value and W_x and W_y are parameters related to the beam width, $W_x = \sqrt{2}\alpha_{sx}$ and $W_y = \sqrt{2}\alpha_{sy}$, with A , W_{s_x} and $W_{s_y} \in \Re$. Defining the relevant parameters in Eq. (3.1) as

$$\begin{aligned}
N &= 1, A_\ell = 2E_0\alpha_{sx}\alpha_{sy}, T_r = 1, \gamma_3 = 0, c_1 = 1, c_2 = 1, d_1 = 2, d_2 = 2, \\
A &= 2, F_3 = 0, m_i = 0, V_{x\ell} = 0, V_{y\ell} = 0,
\end{aligned}
\tag{3.34}$$

Lorentz beam is obtained. After substitution of Eq. (3.34) into Eq. (3.1), Eq. (3.2) and Eq. (3.3), the general beam source equation reduces to

$$u(s_x, s_y, 0) = 2E_0\alpha_{sx}\alpha_{sy} \frac{1}{(2\alpha_{sx}^2 + s_x^2)(2\alpha_{sy}^2 + s_y^2)},
\tag{3.35}$$

which is the Lorentz beam source equation [35]. The intensity is calculated from Eq. (3.4) and Fig. (3-7) is the intensity distribution of Lorentz beam at the source plane.

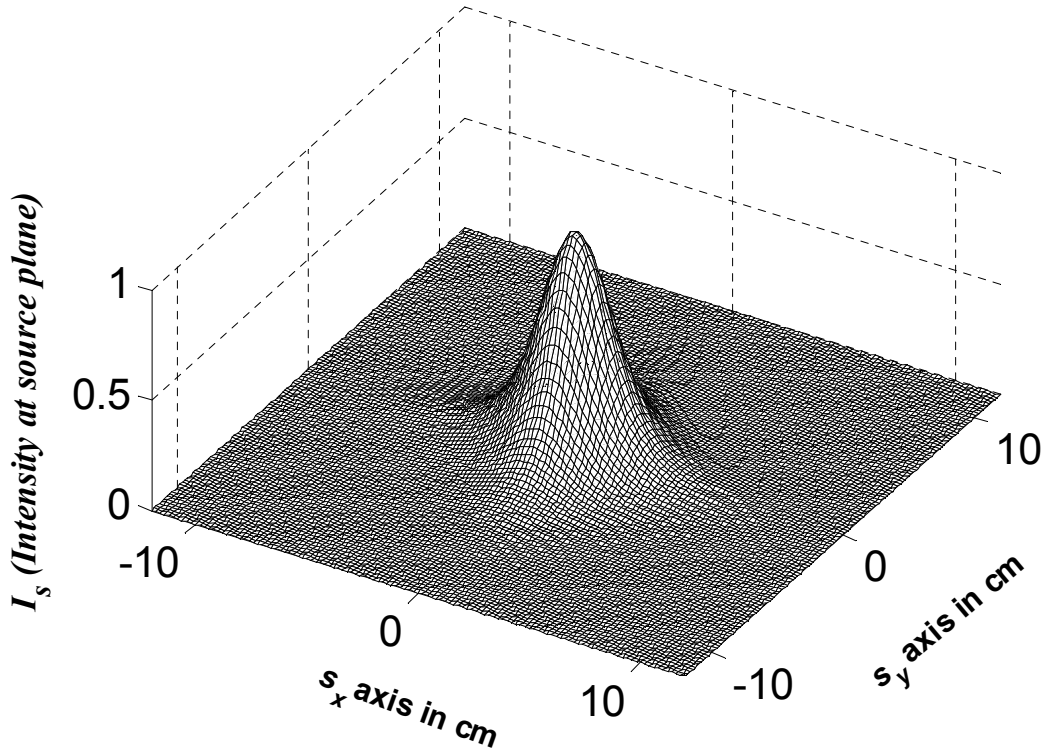


Figure 3-7 Lorentz beam intensity at the source plane.

3.1.11 Hermite-sinusoidal-Gaussian Beams

Hermite-sinusoidal-Gaussian beams are the general form of the beams whose special cases cover a big range of beam types such as Hermite-cosh-Gaussian, Hermite-sinh-Gaussian, Hermite-cos-Gaussian, Hermite-sine-Gaussian, cosh-Gaussian, sinh-Gaussian, cos-Gaussian and sine-Gaussian.

The field at the source plane for the off-axis Hermite-sinusoidal-Gaussian beam is written as

$$\begin{aligned}
 u(s_x, s_y, 0) = & \sum_{\ell=1}^2 A_{\ell} H_{n_{\ell}}(a_{x\ell}s_x + b_{x\ell}) H_{m_{\ell}}(a_{y\ell}s_y + b_{y\ell}) \\
 & \times \exp\left[-\frac{1}{2}\left(\frac{s_x^2}{\alpha_{sx}^2} + \frac{s_y^2}{\alpha_{sy}^2}\right)\right] \exp\left[-j(V_{x\ell}s_x + V_{y\ell}s_y)\right] \\
 & \times \exp(-j\theta_{\ell}), \tag{3.36}
 \end{aligned}$$

where

$$\begin{aligned}
 A_1 = A_0j, A_2 = -A_0j, \theta_{\ell} = \theta, \alpha_{sx} = \alpha, \alpha_{sy} = \alpha, \\
 n_{\ell} = n, m_{\ell} = m, V_{x1} = V_0, V_{x2} = -V_0, V_{y1} = V_0, V_{y2} = -V_0. \tag{3.37}
 \end{aligned}$$

Defining the relevant parameters in Eq. (3.1) as

$$\begin{aligned}
 N = 2, A_1 = A_0j, A_2 = -A_0j, T_r = 1, \gamma_3 = 0, c_1 = 0, \\
 c_2 = 0, A = 0, B = 0, C = 0, G = -1, H = \frac{1}{2}, F_4 = 2, \\
 J = \frac{1}{2}, F_5 = 2, F_3 = 1, m_2 = 1, \phi = \theta, \alpha_{sx} = \alpha, \alpha_{sy} = \alpha, \\
 n_{\ell} = n, m_{\ell} = m, V_{x1} = V_0, V_{x2} = -V_0, V_{y1} = V_0, V_{y2} = -V_0, \tag{3.38}
 \end{aligned}$$

Hermite-sinusoidal-Gaussian beam source equation is obtained. Substituting Eq. (3.38) into Eq. (3.1), the reduced form of general beam source equation yields Hermite-sinusoidal-Gaussian beam. Eq. (3.36) represented by the superposition of two fields (with different complex displacement parameters) for the off-axis

Hermite Gaussian beams. This superposition yields a field at the source plane for the geeralized Hermite- sinusoidal-Gaussian beam. Other beams such as Hermite-sine-Gaussian, Hermite-sinh-Gaussian, Hermite-cos-Gaussian and Hermite-cosh-Gaussian can be derived from this source equation. Table 3-1 is the parameter table that shows which parameter is used for the different beams.

Table 3-1 Parameters for Hermite Gaussian Beams

Parameters	Hermite-sine-Gaussian Beam	Hermite-sinh-Gaussian Beam	Hermite-cos-Gaussian Beam	Hermite-cosh-Gaussian Beam
(V_{x1}, V_{x2})	$(V_0, -V_0)$	$(V_0j, -V_0j)$	$(V_0, -V_0)$	$(V_0j, -V_0j)$
(V_{y1}, V_{y2})	$(V_0, -V_0)$	$(V_0j, -V_0j)$	$(V_0, -V_0)$	$(V_0j, -V_0j)$
(A_1, A_2)	$(A_0j, -A_0j)$	$(A_0, -A_0)$	(A_0, A_0)	(A_0, A_0)
(n_1, n_2)	(n, n)	(n, n)	(n, n)	(n, n)
(m_1, m_2)	(m, m)	(m, m)	(m, m)	(m, m)
$(\alpha_{s_{x1}}, \alpha_{s_{x2}})$	(α_s, α_s)	(α_s, α_s)	(α_s, α_s)	(α_s, α_s)

It can be seen from Table (3-1) that for all beams, there exists $x - y$ symmetry. In this context, n, m are positive integers, α_s and V_0 are positive numeric values conforming to the equalities for Hermite-sine-Gaussian, Hermite-cos-Gaussian, Hermite-sinh-Gaussian and Hermite-cosh-Gaussian beams $n = n_1 = n_2, m = m_1 = m_2, (\alpha_s, \alpha_s) = (\alpha_{s_{x1}}, \alpha_{s_{x2}}) = \alpha_{s_{x2}} = \alpha_{s_{y1}} = \alpha_{s_{y2}}, V_0 = V_{x1} = V_{x2} = V_{y1} = V_{y2}$. Also other fundamental modes such as cos-Gaussian, sine-Gaussian, cosh-Gaussian, sinh-Gaussian and higher order annular beams can be derived from this source formulation with Hermite orders $n = 0, m = 0$. After substitution of Eq. (3.38) into Eq. (3.1), Hermite-sinusoidal-Gaussian beam source equation can be obtained [36]. The intensity can be calculated by using Eq. (3.4). The intensity distribution of Hermite- sinusoidal -Gaussian beam for different parameters such as

$\alpha = 2 \times 10^{-2}$ m, $V_\ell = 120$, $n = 1$, $m = 0$, $\theta = 0$, $A_\ell = 0.5$

can be seen in Fig. (3-8).

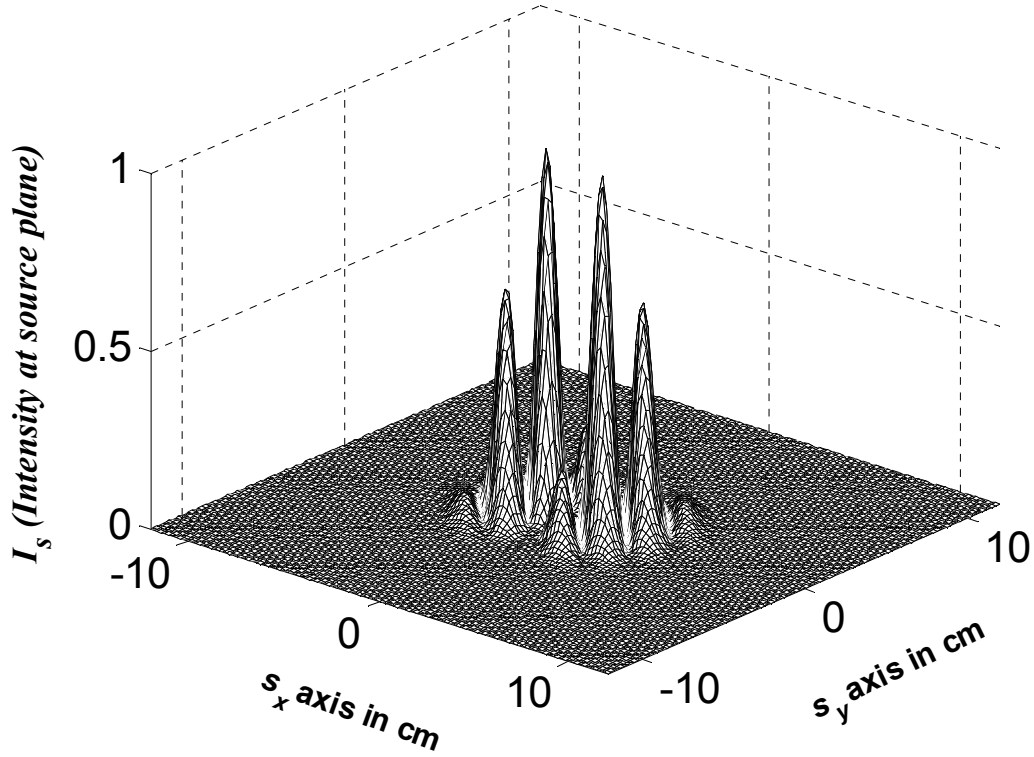


Figure 3-8 Intensity distribution of Hermite-sine-Gaussian beam with $n = 1$, $m = 0$ at the source plane.

3.1.11.1 Hermite-cosh-Gaussian Beam

Hermite-cosh-Gaussian beams can be derived from the Hermite-sinusoidal-Gaussian beams as it is specified above. The source equation can be written as Eq. (3.36). Using Table 3.1 the following parameters can be defined as

$$\begin{aligned} A_1 &= A_0, A_2 = A_0, \alpha_{sx} = \alpha, \alpha_{sy} = \alpha, n_\ell = n, m_\ell = m, \\ V_{x1} &= V_0 j, V_{x2} = -V_0 j, V_{y1} = V_0 j, V_{y2} = -V_0 j, \end{aligned} \quad (3.38)$$

for the Hermite-cosh-Gaussian beam. After substitution of Eq. (3.38) into Eq. (3.36), the formulation turns into Hermite-cosh-Gaussian beam source equation. Also, from the general source beam formulation, with the parameters

$$\begin{aligned}
N &= 2, A_1 = A_0, A_2 = A_0, T_r = 1, \gamma_3 = 0, c_1 = 0, c_2 = 0, A = 0, B = 0, \\
C &= 0, G = -1, H = \frac{1}{2}, F_4 = 2, J = \frac{1}{2}, F_5 = 2, m_2 = 1, \phi = \theta, F_3 = 1, \\
\alpha_{sx} &= \alpha, \alpha_{sy} = \alpha, n_\ell = n, m_\ell = m, V_{x1} = V_0 j, V_{x2} = -V_0 j, V_{y1} = V_0 j, \\
V_{y2} &= -V_0 j,
\end{aligned} \tag{3.39}$$

Eq. (3.36) can be converted to Hermite-cosh-Gaussian beam source equation. Substituting Eq. (3.39) into Eq. (3.1), Eq. (3.2) and Eq. (3.3), the general source beam equation reduces to the Hermite-cosh-Gaussian beam source equation [36].

3.1.11.2 Hermite-cos-Gaussian Beam

Hermite-cos-Gaussian beams also can be derived from Hermite-sinusoidal-Gaussian beams. The source equation can be written as Eq. (3.36). Using Table 3.1 the following parameters can be defined as

$$\begin{aligned}
N &= 2, A_1 = A_0, A_2 = A_0, T_r = 1, \gamma_3 = 0, c_1 = 0, c_2 = 0, A = 0, B = 0, \\
C &= 0, G = -1, H = \frac{1}{2}, F_4 = 2, J = \frac{1}{2}, F_5 = 2, F_3 = 1, m_2 = 1, \phi = \theta, \\
\alpha_{sx} &= \alpha, \alpha_{sy} = \alpha, n_\ell = n, m_\ell = m, V_{x1} = V_0, V_{x2} = -V_0, V_{y1} = V_0, \\
V_{y2} &= -V_0,
\end{aligned} \tag{3.40}$$

for the Hermite-cos-Gaussian beam source equation. Substituting Eq. (3.40) into Eq. (3.1), Eq. (3.2) and Eq. (3.3), the general source beam equation reduces to the Hermite-cos-Gaussian beam source equation [36].

3.1.11.3 Hermite-sinh-Gaussian Beam

Hermite-sinh-Gaussian beams can be derived from Hermite-sinusoidal-Gaussian beams.

The following parameters can be defined as

$$\begin{aligned}
 N &= 2, A_1 = A_0, A_2 = -A_0, T_r = 1, \gamma_3 = 0, c_1 = 0, c_2 = 0, A = 0, B = 0, \\
 C &= 0, G = -1, H = \frac{1}{2}, F_4 = 2, J = \frac{1}{2}, F_5 = 2, F_3 = 1, m_2 = 1, \phi = \theta, \\
 \alpha_{sx} &= \alpha, \alpha_{sy} = \alpha, n_\ell = n, m_\ell = m, V_{x1} = V_0j, V_{x2} = -V_0j, V_{y1} = V_0j, \\
 V_{y2} &= -V_0j,
 \end{aligned} \tag{3.41}$$

for the Hermite-sinh-Gaussian beam [36]. As it is shown in Table (3.1), only $V_{x\ell}, V_{y\ell}, A_\ell, n_\ell, m_\ell$ parameters change.

3.1.11.4 Cos-Gaussian Beam

Cos-Gaussian beams can be derived from the same equation for Hermite-sinusoidal - Gaussian beam. A table can be generated for cos-Gaussian, sine-Gaussian, sinh-Gaussian, cosh-Gaussian.

Table 3-2 Parameters for Sinusoidal Gaussian Beams

Parameters	Cos-Gaussian Beam	Cosh-Gaussian Beam	Sine-Gaussian Beam	Sinh-Gaussian Beam
(V_{x1}, V_{x2})	$(V_0, -V_0)$	$(V_0j, -V_0j)$	$(V_0, -V_0)$	$(V_0j, -V_0j)$
(V_{y1}, V_{y2})	$(V_0, -V_0)$	$(V_0j, -V_0j)$	(m, m)	$(V_0j, -V_0j)$
(A_1, A_2)	(A_0, A_0)	(A_0, A_0)	$(A_0j, -A_0j)$	$(A_0, -A_0)$
(n_1, n_2)	$(0, 0)$	$(0, 0)$	$(0, 0)$	$(0, 0)$
(m_1, m_2)	$(0, 0)$	$(0, 0)$	$(0, 0)$	$(0, 0)$
$(\alpha_{sx1}, \alpha_{sx2})$	(α_s, α_s)	(α_s, α_s)	(α_s, α_s)	(α_s, α_s)

Although there exists $x-y$ symmetry for all Hermite-sinusoidal-Gaussian and sinusoidal-Gaussian beams, for higher-order annular beam there is a different case. For higher-order annular beam $\alpha_{s1} > \alpha_{s2}$.

Using Table (3-2), the following parameters can be defined as

$$\begin{aligned}
N &= 2, A_1 = A_0, A_2 = A_0, T_r = 1, \gamma_3 = 0, c_1 = 0, c_2 = 0, A = 0, B = 0, \\
C &= 0, G = -1, H = \frac{1}{2}, F_4 = 2, J = \frac{1}{2}, F_5 = 2, F_3 = 1, m_2 = 1, \phi = \theta, \\
\alpha_{sx} &= \alpha, \alpha_{sy} = \alpha, n_\ell = 0, m_\ell = 0, V_{x1} = V_0, V_{x2} = -V_0, V_{y1} = V_0, \\
V_{y2} &= -V_0,
\end{aligned} \tag{3.42}$$

for cos-Gaussian beam. After substituting Eq. (3.42) into Eq. (3.1), Eq. (3.2) and Eq. (3.3), the reduced form of general beam source equation yields the cos-Gaussian beam source equation [37].

3.1.11.5 Cosh-Gaussian Beam

According to the Table 3.2 the following parameters can be defined as

$$\begin{aligned}
N &= 2, A_1 = A_0, A_2 = A_0, T_r = 1, \gamma_3 = 0, c_1 = 0, c_2 = 0, A = 0, B = 0, \\
C &= 0, G = -1, H = \frac{1}{2}, F_4 = 2, J = \frac{1}{2}, F_5 = 2, F_3 = 1, m_2 = 1, \phi = \theta, \\
\alpha_{sx} &= \alpha, \alpha_{sy} = \alpha, n_\ell = 0, m_\ell = 0, V_{x1} = V_0 j, V_{x2} = -V_0 j, V_{y1} = V_0 j, \\
V_{y2} &= -V_0 j,
\end{aligned} \tag{3.43}$$

for cosh-Gaussian beam. After substitution of Eq. (3.43) into Eq. (3.1), reduced form of general source beam equation gives the cosh-Gaussian beam Eq. [38]. It can be derived from cos-Gaussian beam by changing $V_{x\ell}$ and $V_{y\ell}$ and making the rest of the source parameters the same.

3.1.11.6 Sine-Gaussian Beam

The source equation can be derived from cosh-Gaussian beam source equation by changing A_ℓ parameters, and making the rest of the parameters the same.

The following parameters can be defined as

$$\begin{aligned}
 N &= 2, A_1 = A_0j, A_2 = -A_0j, T_r = 1, \gamma_3 = 0, c_1 = 0, c_2 = 0, \\
 A &= 0, B = 0, C = 0, G = -1, H = \frac{1}{2}, F_4 = 2, J = \frac{1}{2}, F_5 = 2, \\
 F_3 &= 1, m_2 = 1, \phi = \theta, \alpha_{sx} = \alpha, \alpha_{sy} = \alpha, n_\ell = 0, m_\ell = 0, V_{x1} = V_0, \\
 V_{x2} &= -V_0, V_{y1} = V_0, V_{y2} = -V_0,
 \end{aligned} \tag{3.44}$$

for sine-Gaussian source beam. After substitution of Eq. (3.44) into Eq. (3.1), Eq. (3.2) and Eq. (3.3), reduced form of general source beam equation yields the sine-Gaussian beam equation [39].

3.1.11.7 Sinh-Gaussian Beam

The source equation can be derived from sine-Gaussian beam source equation by changing A_ℓ , $V_{x\ell}$ and $V_{y\ell}$ parameters, and making the rest of the parameters the same.

The following parameters can be defined as

$$\begin{aligned}
 N &= 2, A_1 = A_0, A_2 = -A_0, T_r = 1, \gamma_3 = 0, c_1 = 0, c_2 = 0, A = 0, \\
 B &= 0, C = 0, G = -1, H = \frac{1}{2}, F_4 = 2, J = \frac{1}{2}, F_5 = 2, F_3 = 1, \\
 m_2 &= 1, \phi = \theta, \alpha_{sx} = \alpha, \alpha_{sy} = \alpha, n_\ell = 0, m_\ell = 0, V_{x1} = V_0j, \\
 V_{x2} &= -V_0j, V_{y1} = V_0j, V_{y2} = -V_0j,
 \end{aligned} \tag{3.45}$$

for sinh-Gaussian source beam. After substituting Eq. (3.45) into Eq. (3.1), Eq. (3.2) and Eq. (3.3), reduced form of general source beam equation gives the sinh-Gaussian beam equation [39].

3.1.11.8 Higher-order Annular Beam

Conventionally the annular beam comprises from the difference of two co-centric beam fields, called primary and secondary. Hence a higher-order annular beam aligned to be at the origin of the source plane oriented to be perpendicular to the axis of propagation, z , will have a field distribution [40], which is Eq. (3.36).

The following parameters can be defined as

$$\begin{aligned}
 N &= 2, A_1 = A_0, A_2 = -A_0, T_r = 1, \gamma_3 = 0, c_1 = 0, c_2 = 0, A = 0, B = 0, \\
 C &= 0, G = -1, H = \frac{1}{2}, F_4 = 2, J = \frac{1}{2}, F_5 = 2, F_3 = 1, m_2 = 1, \phi = \theta \\
 \alpha_{sx1} &= \alpha_{s1}, \alpha_{sx2} = \alpha_{s2}, \alpha_{sy1} = \alpha_{s1}, \alpha_{sy2} = \alpha_{s2}, n_\ell = n, m_\ell = m, V_{x\ell} = 0, \\
 V_{y\ell} &= 0,
 \end{aligned} \tag{3.46}$$

for the higher-order annular beam. Here, $\alpha_{s1} \neq \alpha_{s2}$. After substituting Eq. (3.46) into Eq. (3.1), Eq. (3.2) and Eq. (3.3), reduced form of general source beam equation yields the higher order annular beam equation [40].

3.1.12 Elegant Laguerre Gaussian Beam

The standard and elegant Hermite Gaussian, Laguerre Gaussian and Ince Gaussian beams constitute the three orthogonal and biorthogonal, respectively, complete families of paraxial solutions for the scalar Helmholtz equation. The elegant solutions differ from the standard solutions in that the former contain polynomials with a complex argument, whereas in the latter the argument is real. Elegant Laguerre Gaussian beams form a biorthogonal set with their adjoint set of functions [41].

Elegant Laguerre Gaussian beam source equation can be defined as

$$u(r, \theta, 0) = \left(\frac{r}{W_0} \right)^m L_\ell^m \left(\frac{r^2}{W_0^2} \right) \exp(-jm\theta), \tag{3.47}$$

where $r = \sqrt{s_x^2 + s_y^2}$, L_ℓ^m denotes the Laguerre polynomial with mode orders ℓ and m and W_0 is the width of the beam waist.

The following parameters can be defined as

$$\begin{aligned} \ell = \zeta + 1, \quad A_{lm} &= \frac{(-1)^\zeta (N+m)!}{2^{\zeta+m/2} (\alpha_{sx}^{2\zeta+m} + \alpha_{sy}^{2\zeta+m}) (N-\zeta)! (m+\zeta)! \zeta!}, \\ T_r = 1, \quad P = 1, \quad \gamma_1 = \zeta + m/2, \quad R = 0, \quad \gamma_3 = 1, \quad c_1 = 0, \quad c_2 = 0, \\ A = 0, \quad B = 0, \quad C = 0, \quad G = -1, \quad H = 0.5, \quad J = 0.5, \quad F_4 = 2, \\ F_5 = 2, \quad m_2 = m, \quad \phi = \theta, \quad m_i = 0, \end{aligned} \quad (3.48)$$

for the elegant Laguerre Gaussian beam. Substituting Eq. (3.48) into Eq. (3.1), Eq. (3.2) and Eq. (3.3), reduced form of the general source beam becomes

$$\begin{aligned} E(r, \theta) &= \sum_{\zeta=0}^N \frac{(-1)^\zeta (N+m)! (s_x^2 + s_y^2)^{\zeta+m/2}}{2^{\zeta+m/2} (\alpha_{sx}^{2\zeta+m} + \alpha_{sy}^{2\zeta+m}) (N-\zeta)! (m+\zeta)! \zeta!} \\ &\quad \times \exp\left(-\frac{(s_x^2 + s_y^2)}{2(\alpha_{sx}^2 + \alpha_{sy}^2)} - jm\theta\right), \end{aligned} \quad (3.49)$$

which is the elegant Laguerre Gaussian beam [41].

3.1.13 Elliptical Gaussian Beam

The optical field of the generalized elliptical Gaussian beam can be expressed in tensor form as follows [42]

$$u(s_x, s_y, 0) = \exp\left(-\frac{jk}{2} r^T Q^{-1} r\right), \quad (3.50)$$

where $k = 2\pi/\lambda$ is the wavenumber, λ is the wavelength, r denotes a position vector in a transverse plane given by $r^T = (s_x, s_y)$, and Q^{-1} is the 2×2 complex curvature tensor for the generalized elliptical Gaussian beam given by

$$Q^{-1} = \begin{bmatrix} q_{s_x s_x}^{-1} & q_{s_x s_y}^{-1} \\ q_{s_y s_x}^{-1} & q_{s_y s_y}^{-1} \end{bmatrix}, \text{ with } q_{s_x s_y}^{-1} = q_{s_y s_x}^{-1}. \quad (3.51)$$

The following parameters can be defined as

$$\begin{aligned} N = 1, A_{lmm} = 1, T_r = 1, \gamma_3 = 0, c_1 = 0, c_2 = 0, A = 0, \\ B = 0, C = -1, D = -\frac{jk}{2} q_{s_x s_x}, q_{s_x s_x} = -0.201j, \end{aligned} \quad (3.52)$$

for the elliptical Gaussian beam. After substituting Eq. (3.52) into Eq. (3.1), Eq. (3.2) and Eq. (3.3), reduced form of the general source beam equation gives the elliptical Gaussian beam [42] such that

$$E(\mathbf{r}) = \exp \left\{ -\frac{jk}{2} \left[q_{s_x s_x}^{-1} s_x^2 + q_{s_x s_y}^{-1} s_x s_y + q_{s_x s_y}^{-1} s_x s_y + q_{s_y s_y}^{-1} s_y^2 \right] \right\} \quad (3.53)$$

which is the same form as in Eq. (3.50).

CHAPTER 4

FORMULATION AND RESULTS FOR THE AVERAGE RECEIVED INTENSITY OF GENERAL BEAMS IN ATMOSPHERIC TURBULENCE

The variation of the received average intensity profile along a turbulent path depends on the type of the beam used as incidence. This dependency is investigated by many researchers for various types of beams. In all of the studies, the formulation is developed starting with the intended incidence. In this part, it is managed to combine the formulation of the average received intensity in turbulence for most of the mentioned beams in Chapter 3. Although the general source beam formulation can be used in this part to find the average received intensity in turbulence, because it will be bulky, it is not calculated. Here, a portion of Eq. (3.1) is used to calculate the average received intensity in turbulence. Eq. (4.1) is a part of Eq. (3.1) which satisfies the general beam source equation and can be written as

$$u(\mathbf{s}) = \sum_{\ell=1}^N A_{\ell} \exp(-j\theta_{\ell}) H_{n_{\ell}}(a_{x\ell}s_x + b_{x\ell}) \exp\left(-\frac{s_x^2}{2\alpha_{xx}^2} - \frac{s_y^2}{2\alpha_{yy}^2}\right) \times H_{m_{\ell}}(a_{y\ell}s_y + b_{y\ell}) \exp\left[-(jV_{x\ell}s_x + jV_{y\ell}s_y)\right]. \quad (4.1)$$

The average intensity $\langle I(\mathbf{p}, L) \rangle$, of a general beam on a receiver plane located at L distance away from the source can be written as

$$\langle I(\mathbf{p}, L) \rangle = \langle u(\mathbf{p}, L) u(\mathbf{p}, L)^* \rangle, \quad (4.2)$$

where

$$u(\mathbf{p}, L) = \frac{k}{2j\pi L} \exp(jkL) \int_{-\infty}^{\infty} \int_{-\infty}^{\infty} d^2\mathbf{s} u(\mathbf{s}) \times \exp\left[jk(\mathbf{p} - \mathbf{s})^2 / 2L + \psi(\mathbf{s}, \mathbf{p}) \right] \quad (4.3)$$

and

$$u(\mathbf{p}, L)u(\mathbf{p}, L)^* = \frac{k}{2j\pi L} \exp(jkL) \int_{-\infty}^{\infty} \int_{-\infty}^{\infty} d\mathbf{s}_1^2 u(\mathbf{s}_1) \times \exp\left[jk(\mathbf{p} - \mathbf{s}_1)^2 / 2L + \psi(\mathbf{s}_1, \mathbf{p}) \right] \times \frac{k}{(-2j\pi L)} \exp(-jkL) \int_{-\infty}^{\infty} \int_{-\infty}^{\infty} d\mathbf{s}_2^2 u^*(\mathbf{s}_2) \times \exp\left[-jk(\mathbf{p} - \mathbf{s}_2)^2 / 2L + \psi^*(\mathbf{s}_2, \mathbf{p}) \right]. \quad (4.4)$$

After substituting Eq. (4.4) into Eq. (4.2), the average received intensity can be calculated as

$$\langle I(\mathbf{p}, L) \rangle = \left(\frac{k}{2\pi L} \right)^2 \int_{-\infty}^{\infty} \int_{-\infty}^{\infty} \int_{-\infty}^{\infty} \int_{-\infty}^{\infty} d\mathbf{s}_1^2 d\mathbf{s}_2^2 u(\mathbf{s}_1) u^*(\mathbf{s}_2) \times \exp\left\{ jk\left[(\mathbf{p} - \mathbf{s}_1)^2 - (\mathbf{p} - \mathbf{s}_2)^2 \right] / 2L \right\} \times \left\langle \exp\left[\psi(\mathbf{s}_1, \mathbf{p}) + \psi^*(\mathbf{s}_2, \mathbf{p}) \right] \right\rangle, \quad (4.5)$$

where the ensemble average term within the integrand is

$$\left\langle \exp\left[\psi(\mathbf{s}_1, \mathbf{p}) + \psi^*(\mathbf{s}_2, \mathbf{p}) \right] \right\rangle \cong \exp\left[-\rho_0^{-2} (\mathbf{s}_1 - \mathbf{s}_2)^2 \right], \quad (4.6)$$

with ψ being the fluctuations of the complex amplitude, p_x and p_y are the x and y components of the receiver plane vector \mathbf{p} , such that $\mathbf{p} = (p_x, p_y)$, $\rho_0 = (0.545C_n^2 k^2 L)^{-3/5}$ is the coherence length of a spherical wave propagating in the turbulent medium and C_n^2 is the structure constant. Note that Eq. (4.6) is derived under the quadratic approximation for the Rytov's phase structure function, and

$$\begin{aligned}
u(\mathbf{s}_1)u^*(\mathbf{s}_2) &= \sum_{\ell_1=1}^N \sum_{\ell_2=1}^N A_{\ell_1} A_{\ell_2}^* \exp\left[-j(\theta_{\ell_1} - \theta_{\ell_2})\right] \\
&\quad \times H_{n_{\ell_1}}(a_{x\ell_1} s_{1x} + b_{x\ell_1}) \exp\left[-\left(\frac{s_{1x}^2}{2\alpha_{sx1}^2} + jV_{x\ell_1} s_{1x}\right)\right] \\
&\quad \times H_{m_{\ell_1}}(a_{y\ell_1} s_{1y} + b_{y\ell_1}) \exp\left[-\left(\frac{s_{1y}^2}{2\alpha_{sy1}^2} + jV_{y\ell_1} s_{1y}\right)\right] \\
&\quad \times H_{n_{\ell_2}}^*(a_{x\ell_2} s_{2x} + b_{x\ell_2}) \exp\left[-\left(\frac{s_{2x}^2}{2\alpha_{sx2}^2} - jV_{x\ell_2}^* s_{2x}\right)\right] \\
&\quad \times H_{m_{\ell_2}}^*(a_{y\ell_2} s_{2y} + b_{y\ell_2}) \exp\left[-\left(\frac{s_{2y}^2}{2\alpha_{sy2}^2} - jV_{y\ell_2}^* s_{2y}\right)\right]. \quad (4.7)
\end{aligned}$$

After substituting Eq. (4.6) and Eq. (4.7) into Eq. (4.5) and solving the resulting integral by the repeated use of Eq. (3.462.2) of Ref [43], which is

$$\begin{aligned}
\int_{-\infty}^{\infty} dx x^n \exp(-px^2 + 2qx) &= n! \exp(q^2/p) (\pi/p)^{0.5} (q/p)^n \\
&\quad \times \sum_{r=0}^{\lfloor n/2 \rfloor} p^r / \left[(4q^2)^r (n-2r)! (r)! \right], \quad (4.8)
\end{aligned}$$

the following expression is obtained for the average intensity at the receiver plane

$$\begin{aligned}
\langle I(\mathbf{p}, L) \rangle &= \frac{b^2 \rho_0^4}{\left[\rho_0^4 (a_{sx\ell_1} - jb)(a_{sx\ell_2}^* + jb) - 1 \right]^{1/2}} \\
&\quad \times \frac{E_x E_y S_x S_y}{\left[\rho_0^4 (a_{sy\ell_1} - jb)(a_{sy\ell_2}^* + jb) - 1 \right]^{1/2}}, \quad (4.9)
\end{aligned}$$

where $b = k/2L$, $a_{sx\ell_1} = \frac{1}{2\alpha_{sx1}^2} + 1/\rho_0^2$, $a_{sx\ell_2} = \frac{1}{2\alpha_{sx2}^2} + 1/\rho_0^2$, $a_{sy\ell_1}$ and $a_{sy\ell_2}$ are the y counterparts of $a_{sx\ell_1}$ and $a_{sx\ell_2}$,

$$E_x = \exp \left(- \left\{ \frac{(V_{x\ell_1} + 2bp_x)^2}{4(a_{sx\ell_1} - jb)} + \frac{[\rho_0^2 (V_{x\ell_2}^* + 2bp_x)(a_{sx\ell_1} - jb) - V_{x\ell_1} - 2bp_x]^2}{4(a_{sx\ell_1} - jb)[\rho_0^4 (a_{sx\ell_1} - jb)(a_{sx\ell_2}^* + jb) - 1]} \right\} \right), \quad (4.10)$$

E_y is attained by changing all x subscripts to y in E_x ,

$$\begin{aligned} S_x = & \sum_{\ell_1=1}^N \sum_{\ell_2=1}^N \sum_{\ell_{x1}=0}^{[n_{\ell_1}/2]} \sum_{\ell_{nx1}=0}^{n_{\ell_1}-2\ell_{x1}} \sum_{k_{x1}=0}^{[\ell_{nx1}/2]} \sum_{\ell_{x2}=0}^{[n_{\ell_2}/2]} \sum_{\ell_{nx2}=0}^{n_{\ell_2}-2\ell_{x2}} \sum_{k_{x2}=0}^{[(\ell_{nx1}+\ell_{nx2})/2]} T_{\ell_{x1}} T_{\ell_{x2}} \\ & \times A_{\ell_1} A_{\ell_2}^* \exp[-j(\theta_{\ell_1} - \theta_{\ell_2})] (-j)^{\ell_{nx1}+\ell_{nx2}-2k_{x1}-2k_{x2}} \\ & \times (-1)^{\ell_{x1}+\ell_{x2}} 2^{n_{\ell_1}+n_{\ell_2}-\ell_{x1}-\ell_{x2}-\ell_{nx1}-\ell_{nx2}} (-1)^{\ell_{x1}+\ell_{x2}} 2^{n_{\ell_1}+n_{\ell_2}-\ell_{x1}-\ell_{x2}-\ell_{nx1}-\ell_{nx2}} \\ & \times \binom{n_{\ell_1}}{2\ell_{x1}} \binom{n_{\ell_2}}{2\ell_{x2}} \binom{n_{\ell_1}-2\ell_{x1}}{\ell_{nx1}} \binom{n_{\ell_2}-2\ell_{x2}}{\ell_{nx2}} \frac{(\ell_{nx1})!}{(\ell_{nx1}-2k_{x1})!(k_{x1})!} \\ & \times \frac{(\ell_{nx11}+\ell_{nx2})!}{(\ell_{nx11}+\ell_{nx2}-2k_{x2})!(k_{x2})!} (a_{x\ell_1})^{\ell_{nx1}} (a_{x\ell_2}^*)^{\ell_{nx2}} (b_{x\ell_1})^{n_{\ell_1}-2\ell_{x1}-\ell_{nx1}} \\ & \times (b_{x\ell_2}^*)^{n_{\ell_2}-2\ell_{x2}-\ell_{nx2}} (\rho_0^2)^{\ell_{nx2}} [\rho_0^4 (a_{sx\ell_1} - jb)(a_{sx\ell_2}^* + jb) - 1]^{k_{x2}-\ell_{nx11}-\ell_{nx2}} \\ & \times (a_{sx\ell_1} - jb)^{-\ell_{nx1}+k_{x1}+k_{x2}} (V_{x\ell_1} + 2bp_x)^{\ell_{nx1}-2k_{x1}-\ell_{nx11}} \\ & \times [-\rho_0^2 (V_{x\ell_2}^* + 2bp_x)(a_{sx\ell_1} - jb) + V_{x\ell_1} + 2bp_x]^{\ell_{nx11}+\ell_{nx2}-2k_{x2}}. \end{aligned} \quad (4.11)$$

S_y is constructed by changing all x subscripts to y in S_x given by Eq. (4.8).

$T_{\ell_{xj}} = 1 \times 3 \times \dots (2\ell_{xj} - 1)$ for $\ell_{xj} \neq 0$ where $j = 1, 2$, all appearances in the form of $\begin{pmatrix} B_1 \\ B_2 \end{pmatrix}$

represent binomial coefficients, hence $\begin{pmatrix} B_1 \\ B_2 \end{pmatrix} = B_1! / [(B_1 - B_2)! B_2!]$, ! is the factorial

notation, the square brackets, [], placed in the upper limits of some summations mean that the integral part of the expression within the square brackets is to be taken.

In all the figures, $\langle I_{rN} \rangle$ means that for the average received intensity, the following normalization is applied

$$\langle I_{rN} \rangle = \langle I(\mathbf{p}, L) \rangle / \text{Max}[u(\mathbf{s})u^*(\mathbf{s})], \quad (4.12)$$

where the denominator corresponds to the maximum value of the source plane intensity. In all the figures, I_{sN} refers to $\langle I_{rN} \rangle$ at $L = 0$.

The intensity is calculated and plotted at the source plane in Chapter 3. In this chapter, the average received intensity in atmospheric turbulence is calculated by using Eq. (4.1). Moving away from the source plane, the Hermite-sine-Gaussian, Hermite-cosh-Gaussian, Hermite-cosine-Gaussian, and Hermite-sinh-Gaussian laser beams will keep their original shape for some distance; then because of inevitable spreading, neighboring lobes will start to merge [44].

Fig. (4-1) shows the intensity variation of a Hermite-sine-Gaussian beam along the axis of propagation at the distances of $L = 0$ (source plane), 2, 5, 20 km with the parameters $n = 1$, $m = 0$, $a_x = a_y = 50 \text{ m}^{-1}$, $b_x = b_y = 0$, $\alpha_{sx} = \alpha_{sy} = 2 \text{ cm}$, $A_1 = 0.5j$, $A_2 = -0.5j$, $V_{x1} = V_{y1} = 120 \text{ m}^{-1}$, $V_{x2} = V_{y2} = -120 \text{ m}^{-1}$, $\lambda = 1.55 \text{ }\mu\text{m}$, $C_n^2 = 1 \times 10^{-15} \text{ m}^{-2/3}$. Fig. (4-1) shows that at a distance ($L = 2 \text{ km}$), the beam appears as a sinh-positioned TEM when viewed along the slanted axis [44] which can be shown in Fig. (4-2). As the beam propagates further, the TEM appearance gradually diminishes, turning the beam to a sinh-Gaussian profile as seen in the $L = 20 \text{ km}$ case plot of Fig. (4-1).

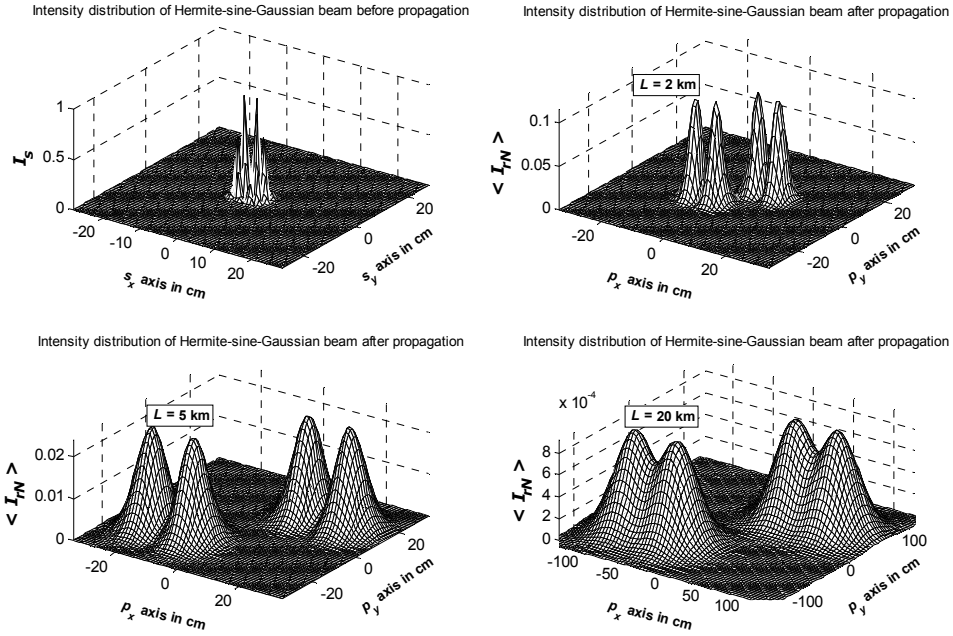


Figure 4-1 Intensity distribution of Hermite-sine-Gaussian beam

$n = 1, m = 0$, at $L=0, 2, 5, 20$ km.

Fig. (4-2) is the intensity distribution of Hermite-cosh-Gaussian beam at source and receiver along the axis of propagation at the distances of $L = 0$ (source plane), 2, 5, 20 km with the parameters $n = 1, m = 0, \lambda = 1.55 \mu\text{m}$, $C_n^2 = 1 \times 10^{-15} \text{ m}^{-2/3}$, $A_1 = 0.5, A_2 = 0.5$, $V_{x1} = V_{y1} = 120j \text{ m}^{-1}$, $V_{x2} = V_{y2} = -120j \text{ m}^{-1}$, $\alpha_{sx} = \alpha_{sy} = 3 \text{ cm}$. It can be seen from Fig. (4-2), with the increasing of propagation distance, the Hermite-cosh-Gaussian beam turns into a pure Gaussian beam [44].

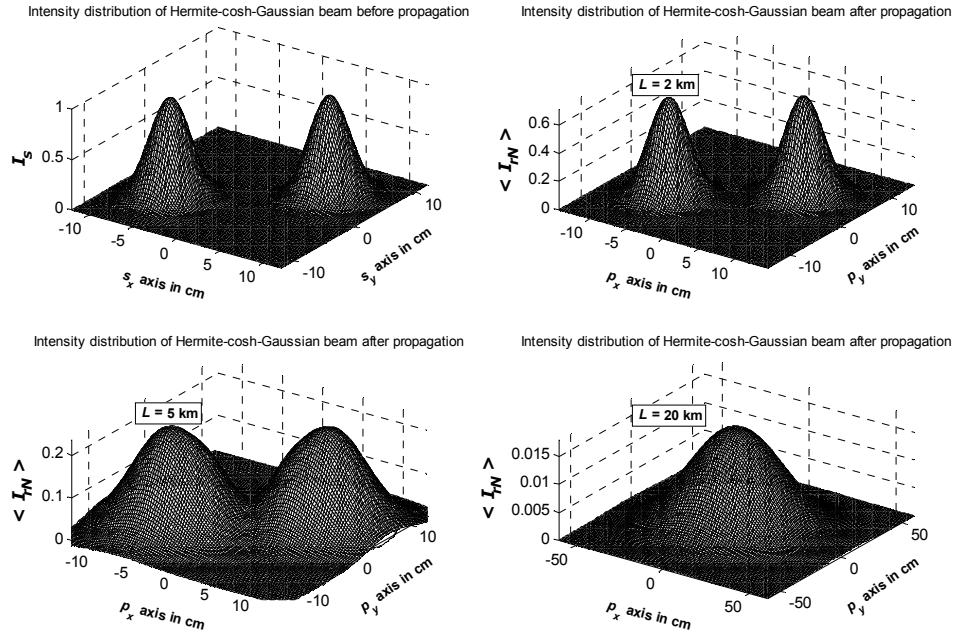


Figure 4-2 Intensity distribution of Hermite-cosh-Gaussian beam with $n = 1, m = 0$, at $L=0, 2, 5, 20$ km.

Fig. (4-3) shows the intensity distribution of a Hermite-cosine-Gaussian beam along the axis of propagation at the distances of $L = 0$ (source plane), 2, 5, 20 km with the parameters $n = 1, m = 1, \lambda = 1.55 \mu\text{m}, C_n^2 = 1 \times 10^{-15} \text{m}^{-2/3}, A_1 = 0.5, A_2 = 0.5, V_{x1} = V_{y1} = 120 \text{m}^{-1}, V_{x2} = V_{y2} = -120 \text{m}^{-1}, \alpha_{xx} = \alpha_{yy} = 2 \text{cm}$. Moving away from the source plane, the Hermite-cosine-Gaussian beam will spread in a way such that some neighboring lobes will start to merge that can be seen from the Fig. (4-3) [45].

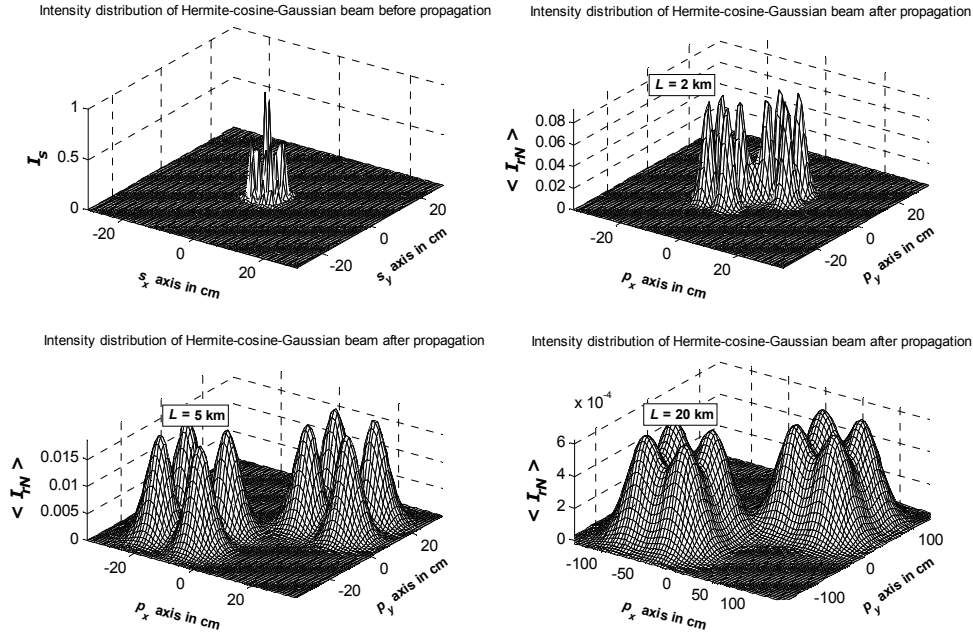


Figure 4-3 Intensity distribution of Hermite-cosine-Gaussian beam with $n = 1, m = 1$, at $L = 0, 2, 5, 20$ km.

Fig. (4-4) shows the intensity distribution of a Hermite-sinh-Gaussian beam along the axis of propagation at the distances of $L = 0$ (source plane), 2, 5, 20 km with the parameters $n = 1, m = 0, \lambda = 1.55 \mu\text{m}, C_n^2 = 1 \times 10^{-15} \text{m}^{-2/3}, A_1 = 0.5, A_2 = -0.5, V_{x1} = V_{y1} = 120j \text{m}^{-1}, V_{x2} = V_{y2} = -120j \text{m}^{-1}, \alpha_{sx} = \alpha_{sy} = 2 \text{cm}$. Here it can be seen for this specific combination of source and medium parameters that the Hermite-sinh-Gaussian beam will produce a pure Gaussian as it propagates a sufficient distance [44]. By comparing Figs. (4-2) and (4-4), it is concluded that a similar intensity pattern is repeated both in the case of Hermite cosh-Gaussian and Hermite-sinh-Gaussian beams. An illustration of a Hermite-sine-Gaussian beam is given in Fig. (4-1) and a Hermite-cosine-Gaussian beam is given in Fig. (4-3). From Figs. (4-1) and (4-3), it is observed that Hermite-sine-Gaussian beam and Hermite-cosine-Gaussian beam have not substantial differences along the propagation path. It is not shown in these plots but Hermite-sine-Gaussian beam and Hermite-cosine-Gaussian beam will turn into a pure Gaussian profile with the increasing distances such as $L = 50$ km.

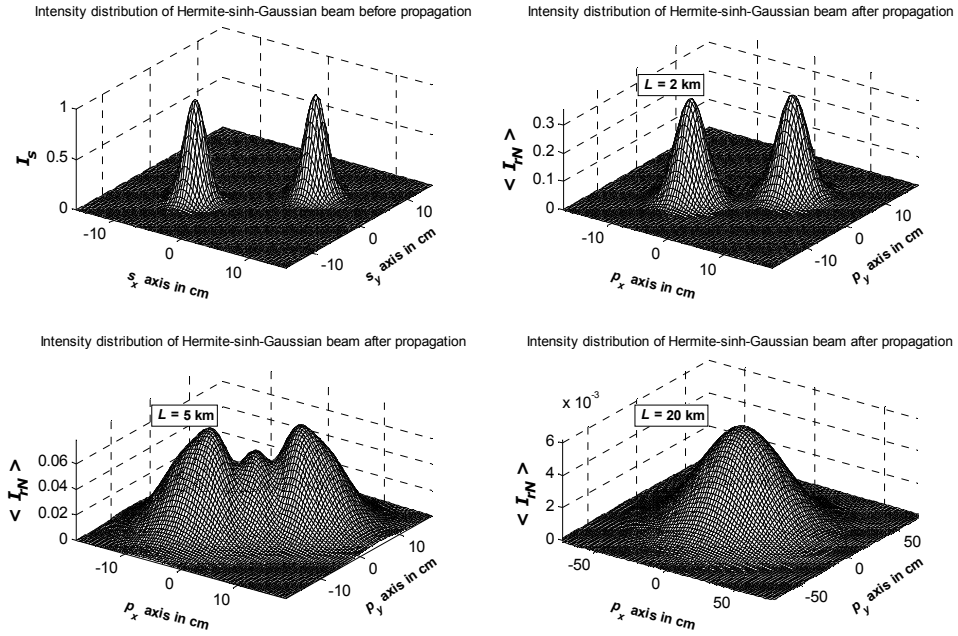


Figure 4-4 Intensity distribution of a Hermite-sinh-Gaussian beam with $n=1$, $m=0$, at $L=0, 2, 5, 20$ km.

Fig. (4-5) is the intensity distribution of a cosine-Gaussian beam at source and receiver along the axis of propagation at the distances of $L=0$ (source plane), 2, 5, 20 km with the parameters $n=0$, $m=0$, $\lambda=1.55 \mu\text{m}$, $C_n^2=1 \times 10^{-15} \text{m}^{-2/3}$, $A_1=0.5$, $A_2=0.5$, $V_{x1}=V_{y1}=50 \text{m}^{-1}$, $V_{x2}=V_{y2}=-50 \text{m}^{-1}$, $\alpha_{sx}=\alpha_{sy}=5 \text{cm}$. With the increasing of propagation distance, the beam spreading can clearly be identified [46]. The upper left and lower left part of Fig. (4-5) show this process.

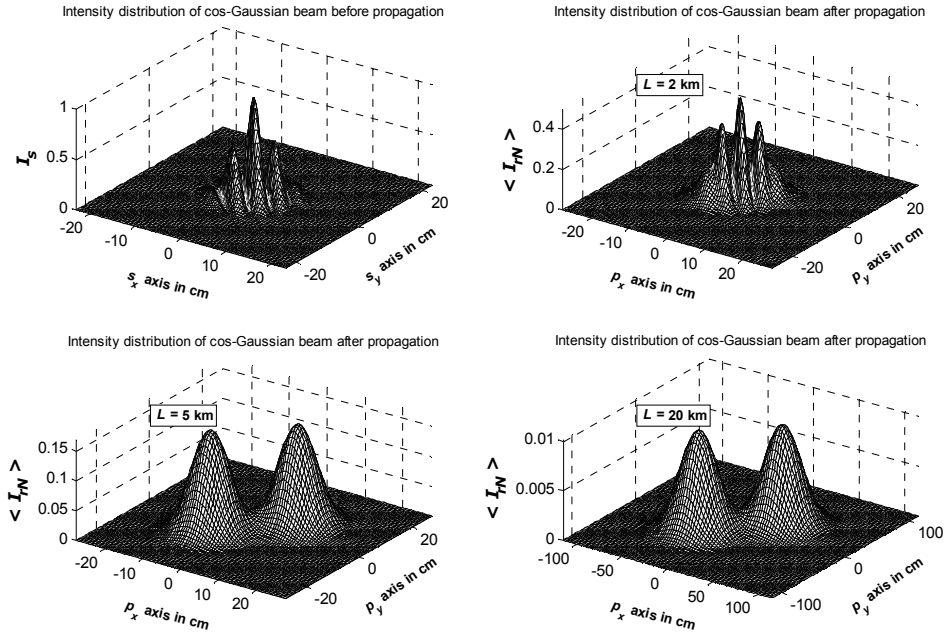


Figure 4-5 Intensity distribution of cosine-Gaussian beam with $n = 0, m = 0$, at $L = 0, 2, 5, 20$ km.

Fig. (4-6) is the progress of a cosh-Gaussian beam along the axis of propagation the distances of $L = 0$ (source plane), 2, 5, 20 km with the parameters $n = 0, m = 0, \lambda = 1.55 \mu\text{m}, C_n^2 = 1 \times 10^{-15} \text{m}^{-2/3}, A_1 = 0.5, A_2 = 0.5, V_{x1} = V_{y1} = 120j \text{m}^{-1}, V_{x2} = V_{y2} = -120j \text{m}^{-1}, \alpha_{sx} = \alpha_{sy} = 2 \text{cm}$. It can be seen from Fig. (4-6), for this specific combination, the cosh-Gaussian beam will produce a pure Gaussian beam with the increasing distances [46].

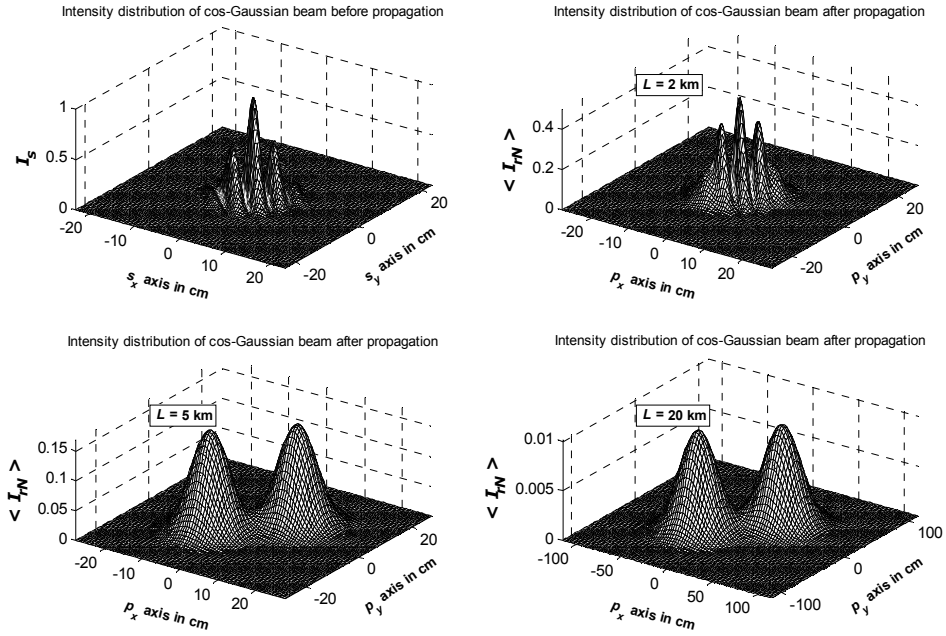


Figure 4-6 Intensity distribution of cosh-Gaussian beam with $n = 0, m = 0$, at $L = 0, 2, 5, 20$ km.

Fig. (4-7) shows the progress of a sine-Gaussian beam along the axis of propagation at the distances of $L = 0$ (source plane), 2, 5, 20 km with the parameters $n = 0, m = 0, a_x = a_y = 50 \text{ m}^{-1}, b_x = b_y = 0, \alpha_{xx} = \alpha_{yy} = 2 \text{ cm}, A_1 = 0.5j, A_2 = -0.5j, V_{x1} = V_{y1} = 120 \text{ m}^{-1}, V_{x2} = V_{y2} = -120 \text{ m}^{-1}, \lambda = 1.55 \mu\text{m}, C_n^2 = 1 \times 10^{-15} \text{ m}^{-2/3}$ [44].

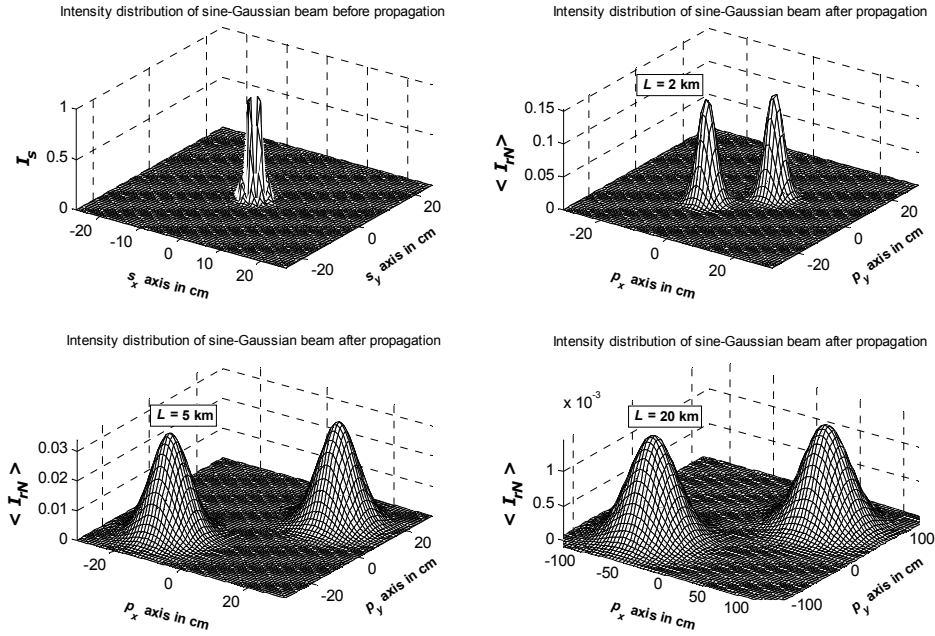


Figure 4-7 Intensity distribution of a sine-Gaussian beam with $n = 1, m = 0$, at $L = 0, 2, 5, 20$ km.

Fig. (4-8) shows the intensity distribution of sinh-Gaussian beam at source and receiver with different distances such as $L = 0, 2, 5, 20$ km with parameters $n = 0, m = 0, a_x = a_y = 50 \text{ m}^{-1}, b_x = b_y = 0, \alpha_{sx} = \alpha_{sy} = 2 \text{ cm}, A_1 = 0.5, A_2 = -0.5, V_{x1} = V_{y1} = 120j \text{ m}^{-1}, V_{x2} = V_{y2} = -120j \text{ m}^{-1}, \lambda = 1.55 \mu\text{m}, C_n^2 = 1 \times 10^{-15} \text{ m}^{-2/3}$ [44]. The sine-Gaussian, cosine-Gaussian, sinh-Gaussian and cosh-Gaussian beams are obtained by taking the parameters as $n = 0$ and $m = 0$. It can be seen from the Figs. (4-6) and (4-8) both cosh-Gaussian and sinh-Gaussian beams will turn into a pure Gaussian profile at $L = 20$ km.

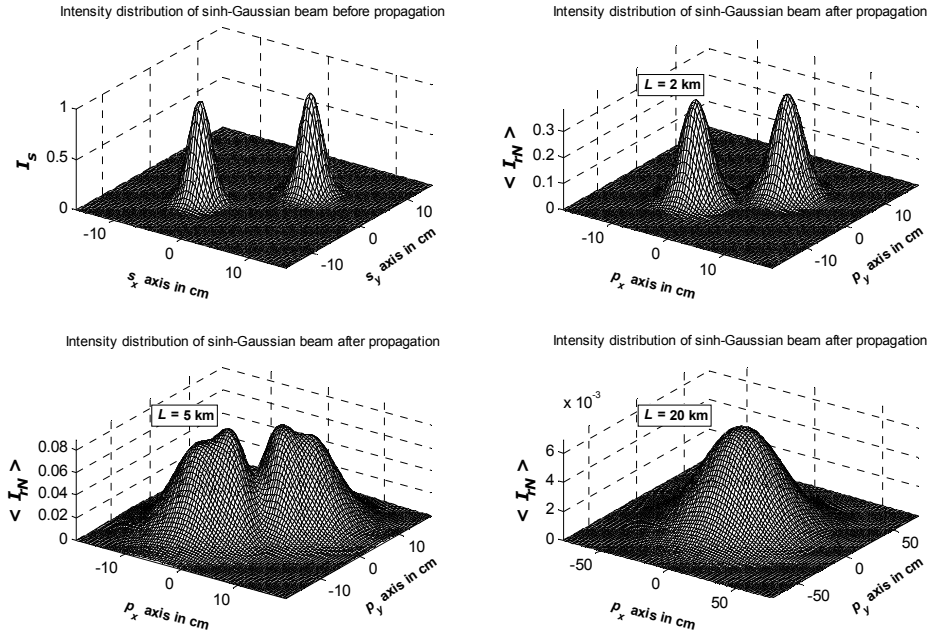


Figure 4-8 Intensity distribution of a sinh-Gaussian beam with $n = 0, m = 0$, at $L = 0, 2, 5, 20$ km.

Fig. (4-9) shows the intensity distribution of annular beam at source and receiver at the distances of $L = 0$ (source plane), 2, 5, 20 km with the parameters $n = 0, m = 0, \lambda = 1.55 \mu\text{m}, C_n^2 = 1 \times 10^{-15} \text{ m}^{-2/3}, V_{x1} = V_{y1} = V_{x2} = V_{y2} = 0, \alpha_{sx1} = \alpha_{sy1} = 3 \text{ cm}, \alpha_{sx2} = \alpha_{sy2} = 1.5 \text{ cm}, A_1 = 0.5, A_2 = -0.5$. It can be seen from Fig. (4-9), with the increasing propagation distances, the annular beam will settle down to a pure Gaussian shape at $L = 20$ km [47].

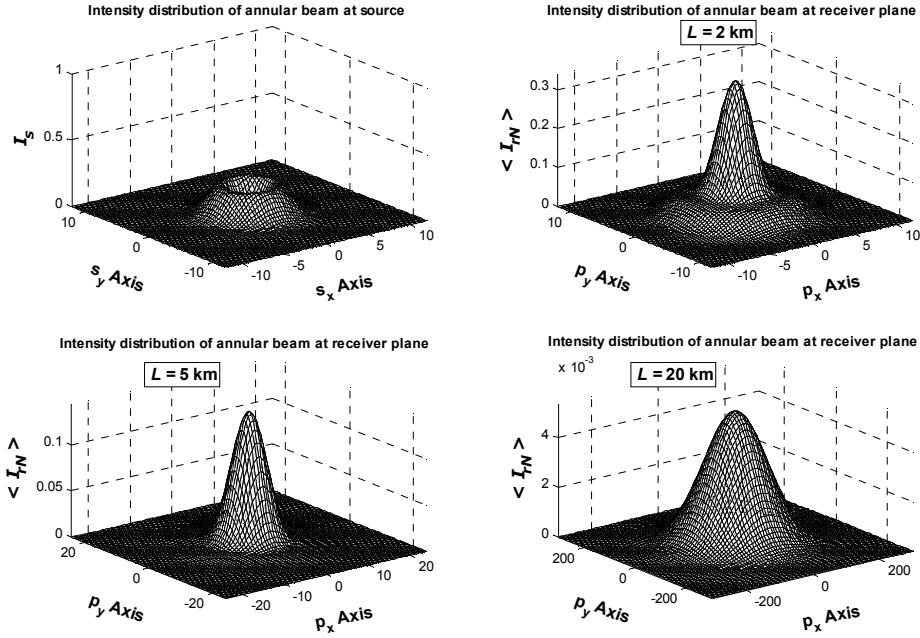


Figure 4-9 Intensity distribution of annular beam with $n = 0, m = 0$, at $L = 0, 2, 5, 20$ km.

Fig. (4-10) shows the intensity distribution of higher order annular beam at source and receiver at the distances of $L = 0$ (source plane), 2, 5, 20 km with the parameters $n = 1, m = 0, \lambda = 1.55 \mu\text{m}, C_n^2 = 1 \times 10^{-15} \text{ m}^{-2/3}, V_{x1} = V_{y1} = V_{x2} = V_{y2} = 0, \alpha_{sx1} = \alpha_{sy1} = 3 \text{ cm}, \alpha_{sx2} = \alpha_{sy2} = 1.5 \text{ cm}, A_1 = 0.5, A_2 = -0.5$. Fig. (4-10) shows that the higher order annular beam will first act to enlarge the initially smaller lobes near on-axis, then the profile will turn into a pure Gaussian shape [47]. Although annular beam turns into a pure Gaussian profile at $L = 20$ km, the higher order annular beam turns into a pure Gaussian profile at a longer propagation distance.

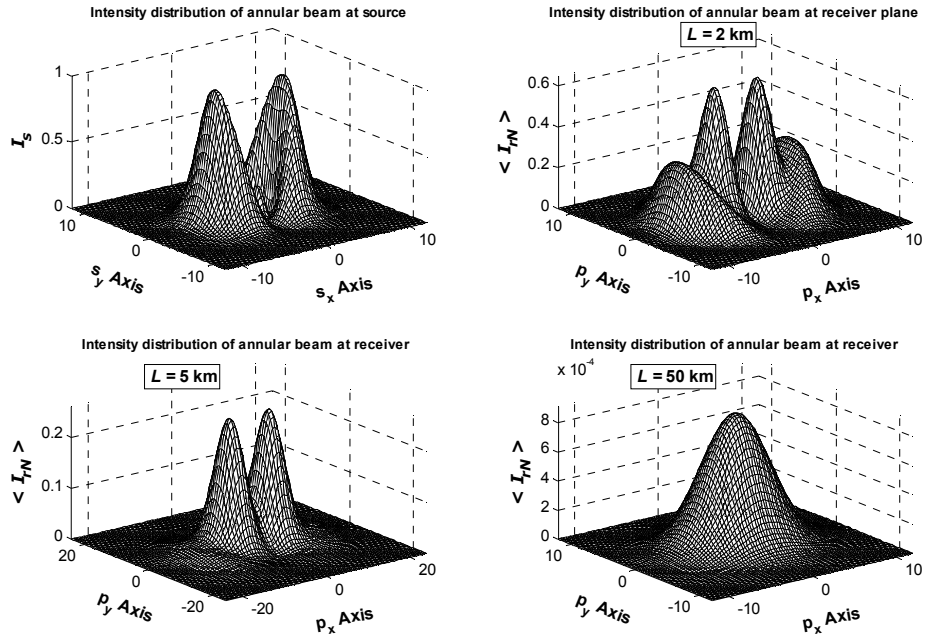


Figure 4-10 Intensity distribution of a higher order annular beam with $n = 1, m = 0$, at $L = 0, 2, 5, 20$ km.

CHAPTER 5

CONCLUSIONS

A formulation is developed to represent a general source beam to combine many types of different beams such as Bessel, Bessel Gaussian, Laguerre, Laguerre Gaussian, Ince Gaussian, dark hollow, bottle, super Gaussian, Lorentz, flat-topped, Hermite-sinusoidal-Gaussian, sinusoidal-Gaussian like cos-Gaussian, sine-Gaussian, cosh-Gaussian, sinh-Gaussian, annular and their higher order modes with their truncated, elegant and elliptical versions in a single expression. With this general source beam formulation, all the mentioned beams' source equations are obtained, compared with their existing forms in the literature and intensity patterns of some of them are plotted at source plane.

Then, using a simplified version of the developed general beam formula, received average intensity is calculated in the presence of atmospheric turbulence. Distributions of the average intensity patterns are obtained at the receiver plane of horizontal atmospheric links specifically for Hermite-sinusoidal-Gaussian, sinusoidal-Gaussian, annular beams and their higher order modes. Variation of the average received intensity profiles for such beams are examined at different propagation distances in atmospheric turbulence. In our formulation, extended Huygens-Fresnel diffraction integral is used. The normalized average intensity distribution is plotted for each beam at different distances as quartet plots, first plot showing the intensity distribution at the source plane, the next three exhibiting the average intensity distributions at different propagation distances.

While Hermite-sinusoidal-Gaussian beams are propagating in turbulence, they keep their original shape for a certain propagation distance, then additional lobes start to

appear. For a sufficient distance, Hermite-sinusoidal-Gaussian beams turn into a Gaussian profile. It can be said that Hermite-sinh-Gaussian beams and Hermite-cosh-Gaussian beams have similar average intensity profiles and at sufficient distances, they turn into Gaussian profile. Hermite-sine-Gaussian and Hermite-cosine-Gaussian beams take Gaussian shape at long propagation distances as compared to the Hermite-sinh-Gaussian and Hermite-cosh-Gaussian beams. For the sinh-Gaussian and cosh-Gaussian beams, because of spreading, neighboring lobes start to merge. At sufficient distance, their average intensity profiles again attain pure Gaussian shapes. Sine-Gaussian beams and cosine-Gaussian beams take Gaussian profile at a longer propagation distances when compared with the sinh-Gaussian and cosh-Gaussian beams. It is interesting to note that the cos-Gaussian beam transforms into cosh-Gaussian beam after propagation in turbulence.

REFERENCES

- [1] <http://cc.ee.ntu.edu.tw/~kpho/u3470/fso.pdf>
- [2] <http://www.free-space-optics.org/>
- [3] **DURNIN, J.** (1987), *Exact Solutions for Nondiffracting Beams*, J. Opt. Soc. Am. A, 651-654. Vol. 4.
- [4] **KOGELNIK, H., LI, H.** (1966), *Laser Beams and Resonators*, Applied Optics, 1550-1567. Vol. 5.
- [5] **BANDRES M.A., VEGA, J.C.** (2004), *Ince-Gaussian Beams*, Optics Letters, 144-146. Vol. 29.
- [6] **YIN, J.** et. al. (1998), *Optical Potential for Atom Guidance in a Dark Hollow Laser Beam*, J. Opt. Soc. Am. B, 25-33. Vol. 15.
- [7] **ARLT, J., PADGETT, M.J.** (2000), *Generation of a Beam With a Dark Focus Surrounded by Regions of Higher Intensity: The Optical Bottle Beam*, Optics Letters, 191-193. Vol. 25.
- [8] **JIANG, Z.** (1997), *Truncation of a Two-Dimensional Nondiffracting cos Beam*, J. Opt. Soc. Am. A, 1478-1481. Vol. 14.
- [9] **GAWHARY, O.E., SEVERINI, S.** (2006), *Lorentz Beams*, J. Opt. A: Pure Appl. Opt., 406-414. Vol.8.
- [10] **GORI, F.** (1994), *Flattened Gaussian Beams*, Opt. Commun., 335-341. Vol. 107.

- [11] **SAGHAFI, S., SHEPPARD, J. R.** (1998), *Near Field and Far Field of Elegant Hermite-Gaussian and Laguerre-Gaussian Modes*, J. Mod. Opt., 1999–2009. Vol. 45.
- [12] **LIN, Q.** et. al. (1990), *Transformation of Non-Symmetric Gaussian Beam Into Symmetric One by Means of Tensor ABCD Law*, Optik (Stuttgart) 67-72. Vol. 85.
- [13] **ARPALI, Ç.** et. al. (2006), *Simulator for General-Type Beam Propagation in Turbulent Atmosphere*, Opt. Express, 8918-8928. Vol. 14.
- [14] **SMITH, F.G.** (1993), *Atmospheric Propagation of Radiation*, SPIE Press, Bellingham, Washington.
- [15] **ANDREWS, L. C.** (2004), *Field Guide to Atmospheric Optics*, SPIE Press, Bellingham, Washington.
- [16] no author
LMDS Versus Free-Space Optical Networks (2001), Light Pointe.
- [17] **SZEBESTA, D.** (2002), *Free Space Optical Communication*, Colt Telecommunications, London.
- [18] **SALEH, B. E. A., TEICH, M.C.** (1991), *Fundamentals of Photonics*, John Wiley & Sons, Inc.
- [19] <http://www.ast.cam.ac.uk>
- [20] **ZHU, X., KAHN, J. M., WANG, J.** (2003), *Mitigation of Turbulence-Induced Scintillation Noise in Free-Space Optical Links Using Temporal-Domain Detection Techniques*, IEEE Photonics Technology Letters, 623-625. Vol. 15.
- [21] **ZHU, X., KAHN, J.M** (2003), *Performance Bounds for Coded Free-Space Optical Communications Through Atmospheric Turbulence Channels*, IEEE Transactions on Communications, 1233-1239. Vol. 51.

- [22] **TYSON, R.K.** (1991), *Principles of Adaptive Optics*, Academic Press, Inc.
- [23] **KRAVTSOV, Y. A.** (1992), *Propagation of Electromagnetic Waves Through a Turbulent Atmosphere*, Rep. Prog. Phys., 39-112.
- [24] **LUTOMIRSKI, R. F., YURA, H. T.** (1974), *Imaging of Extended Objects Through a Turbulent Atmosphere*, Applied Optics, 431-437. Vol. 13.
- [25] **ANDREWS, L. C.** (1998), *Special Functions of Mathematics for Engineers*, Oxford University Press.
- [26] **MC QUEEN, C. A., ARLT, J., DHOLAKIA K.** (1999), *An Experiment to Study A "Nondiffracting" Light Beam*, Am. J. Phys., 912-915. Vol. 67.
- [27] **JORDAN, R. H., HALL, D.G.** (1993), *Free-Space Azimuthal Paraxial Wave Equation: The Azimuthal Bessel-Gauss Beam Solution*, Optics Letters, 427-429. Vol. 19.
- [28] **ZHANG, W., KUZYK, M.G.** (2006), *Effect of a Thin Optical Kerr Medium On A Laguerre-Gaussian Beam*, Applied Physics Letters, 101103(1)-101103(3). Vol. 89.
- [29] **BANDRES, M., VEGA, J. C. G.** (2005), *Ince-Gaussian Two-dimensional Fractional Fourier Transform for Optical Wave Propagation*, SPIE, 321. Vol. 5876.
- [30] **MEI, Z., ZHAO, D.** (2005), *Controllable Dark-Hollow Beams And Their Propagation Characteristics*, J. Opt. Soc. Am. A, 1898-1902. Vol. 22.
- [31] **ARLT, J., PADGETT, M.J.** (2000), *Generation of a beam with a dark focus surrounded by regions of higher intensity: the optical bottle beam*, Optics Letters, 191-193. Vol. 25.

- [32] **FREEGARDE, T., DHOLAKIA, K.** (2002), *Cavity Enhanced Optical Bottle Beam As a Mechanical Amplifier*, Physical Review A., 013413. Vol. 66.
- [33] **DICKEY, F.M., HOLSWADE, S.C.** (2000), *Laser Beam Shaping: Theory and Techniques*.
- [34] **ZHIPING, J.** (1997), *Truncation of A Two Dimensional cos Beam*, J. Opt. Soc. Am. A., 1478-1481. Vol. 14.
- [35] **GAWHARY, O.E., SEVERINI, S.** (2006), *Lorentz Beams*, J. Opt. A: Pure Appl. Opt., 409. Vol. 8.
- [36] **EYYUBOGLU, H.T., BAYKAL, Y.** (2005), *Hermite-sin-Gaussian and Hermite-sinh-Gaussian Laser Beams in Turbulent Atmosphere*, J. Opt. Soc. Am. A., 2709- 2718. Vol. 22.
- [37] **EYYUBOGLU, H.T., BAYKAL, Y.** (2004), *Analysis of Reciprocity of cos-Gaussian and cosh-Gaussian Laser Beams in Turbulent Atmosphere*, Optics Express, 4659-4674. Vol. 12.
- [38] **EYYUBOGLU, H.T., BAYKAL, Y.** (2005), *Average Intensity and Spreading of cosh-Gaussian Laser Beams in the Turbulent Atmosphere*, Appl. Opt, 976-983. Vol. 44.
- [39] **FEIZULIN, Z.I., KRAVTSOV, Y.** (1967), *Broadening of A Laser Beam in A Turbulent Medium*, Quantum Electron, 33-35. Vol. 10.
- [40] **EYYUBOĞLU, H. T., ALTAY, S., BAYKAL, Y.** (2006), *Propagation Characteristics of Higher-Order Annular Gaussian Beams in Atmospheric Turbulence*, Opt. Commun., 25-34. Vol. 264.
- [41] **MEI, Z., ZHAO, D.** (2004), *Propagation of Laguerre-Gaussian and elegant Laguerre-Gaussian beams in apertured fractional Hankel transform systems*, Opt. Soc. Am. A, 2375-2381. Vol. 21.

- [42] **YANGJIAN, C., LIN, Q.** (2002), *Decentered Elliptical Gaussian Beam*, Applied Optics, 4336-4340. Vol. 41.
- [43] **GRADSHTEYN, I.S., RYZHIK, I.M.** (2000), *Tables of Integrals, Series and Products*, Academic Press, New York.
- [44] **EYYUBOĞLU, H.T., BAYKAL, Y.** (2005), *Hermite-sine-Gaussian and Hermite-sinh-Gaussian Laser Beams in Turbulent Atmosphere*, J. Opt. Soc. Am. A., 2709-2718. Vol. 22.
- [45] **EYYUBOĞLU, H. T.** (2005), *Hermite-cosine-Gaussian Laser Beam and Its Propagation Characteristics in Turbulent Atmosphere*, J. Opt. Soc. Am. A., 1527- 1535. Vol. 22.
- [46] **EYYUBOĞLU, H.T., BAYKAL, Y.** (2004), *Analysis of Reciprocity of cos-Gaussian and cosh-Gaussian Laser Beams in a Turbulent Atmosphere*, Optics Express, 4659- 4674. Vol. 12.
- [47] **EYYUBOĞLU, H. T., ALTAY, S., BAYKAL, Y.** (2006), *Propagation Characteristics of Higher-order Annular Gaussian Beams in Atmospheric Turbulence*, Optics Communications, 25-34. Vol. 264.